1 **The development of ovine gastric and intestinal organoids for studying ruminant host-**
2 **pathogen interactions**

3

4 **David Smith[1][*][**]; Daniel R. G. Price[1][*]; Alison Burrells[1]; Marc N. Faber[1]; Katie A.**
5 **Hildersley[1,2]; Cosmin Chintoan-Uta[3]; Ambre F. Chapuis[1, 3]; Mark Stevens[3], Karen**
6 **Stevenson[1]; Stewart T. G. Burgess[1]; Elisabeth A. Innes[1]; Alasdair J. Nisbet[1]; Tom N.**
7 **McNeilly[1]**
8
9 [*]co-first authors
10 [1]Moredun Research Institute, Pentlands Science Park, Midlothian, United Kingdom EH26 0PZ
11 [2]Institute of Biodiversity, Animal Health and Comparative Medicine, University of Glasgow,
12 United Kingdom G61 1QH
13 [3]The Roslin Institute, University of Edinburgh, Midlothian, United Kingdom EH25 9RG
14 [**]**Correspondence: d.smith@moredun.ac.uk**

15

16 **Keywords:** mini-guts, three-dimensional (3D) organoids, host-pathogen interactions, *in vitro*
17 culture systems, stem cells, crypts, sheep, gastrointestinal

18

19 **Abstract**
20 Gastrointestinal (GI) infections in sheep have significant implications for animal health,
21 welfare and productivity, as well as being a source of zoonotic pathogens. Interactions between
22 pathogens and epithelial cells at the mucosal surface play a key role in determining the outcome
23 of GI infections; however, the inaccessibility of the GI tract *in vivo* significantly limits the
24 ability to study such interactions in detail. We therefore developed ovine epithelial organoids
25 representing physiologically important gastric and intestinal sites of infection, specifically the
26 abomasum (analogous to the stomach in monogastrics) and ileum. We show that both abomasal
27 and ileal organoids form self-organising three-dimensional structures with a single epithelial
28 layer and a central lumen that are stable in culture over serial passage. We performed RNA-
29 seq analysis on abomasal and ileal tissue from multiple animals and on organoids across
30 multiple passages and show the transcript profile of both abomasal and ileal organoids cultured
31 under identical conditions are reflective of the tissue from which they were derived and that
32 the transcript profile in organoids is stable over at least five serial passages. In addition, we
33 demonstrate that the organoids can be successfully cryopreserved and resuscitated, allowing
34 long-term storage of organoid lines, thereby reducing the number of animals required as a
35 source of tissue. We also report the first published observations of a helminth infecting gastric
36 and intestinal organoids by challenge with the sheep parasitic nematode *Teladorsagia*
37 *circumcincta*, demonstrating the utility of these organoids for pathogen co-culture experiments.
38 Finally, the polarity in the abomasal and ileal organoids can be inverted to make the apical
39 surface directly accessible to pathogens or their products, here shown by infection of apical-
40 out organoids with the zoonotic enteric bacterial pathogen *Salmonella enterica* serovar
41 Typhimurium. In summary, we report a simple and reliable *in vitro* culture system for
42 generation and maintenance of small ruminant intestinal and gastric organoids. In line with 3Rs
43 principals, use of such organoids will reduce and replace animals in host-pathogen research.
44

45 **1. Introduction**
46 The mammalian gastrointestinal (GI) tract is the site of digestion and nutrient absorption, as
47 well as a predilection site for many infectious pathogens, including bacteria, viruses and
48 parasites. Understanding how pathogens attach and invade cells in the GI tract will help

49    determine mechanisms of host infection, disease pathogenesis and enable strategies to prevent
50    and control infectious disease. Both the gastric stomach and intestine share a number of
51    common features, including a single luminal layer of epithelial cells sealed by tight junctions
52    which is renewed approximately every 3 – 5 days. In both organs, this huge regenerative
53    capacity is mediated by proliferation and differentiation of tissue resident adult stem cells
54    (ASCs) (Barker et al., 2007, 2010; Sato et al., 2009; Xiao and Zhou, 2020). In intestinal tissues,
55    pockets of leucine-rich repeat-containing G protein-coupled receptor 5 (LGR5)-expressing
56    ASCs reside in the base of the crypts of Lieberkühn and can differentiate into all five epithelial
57    cell types of the intestine: enterocytes, goblet cells, enteroendocrine cells, tuft cells, and Paneth
58    cells (Barker et al., 2007; Sato et al., 2009). In the stomach the epithelia is arranged into
59    multiple gastric units, which comprise of the gastric pit, isthmus, neck and base with
60    proliferative stem cells located in the isthmus (Barker et al., 2010; Xiao and Zhou, 2020). The
61    ASCs of the gastric gland can differentiate into all five epithelial cell types of the gastric
62    stomach: surface neck mucus cells, parietal cells, chief cells, enteroendocrine cells (including
63    G cells, D cells, and enterochromaffin-like cells) and tuft cells (Barker et al., 2010; Xiao and
64    Zhou, 2020).

65    The huge regenerative capacity of GI tract and the ability of ASCs to differentiate into
66    epithelial cell types present in the GI tract has been exploited to develop GI organoids or "mini-
67    guts" that reflect the cellular diversity and physiology of the organ from which they were
68    derived (Sato et al., 2009; Barker et al., 2010). Organoid models of the GI tract were first
69    developed from mouse stomach and intestine tissues. To achieve this, researchers isolated
70    mouse LGR5$^+$ adult stem cells from these organs and cultured them in a laminin rich
71    extracellular matrix extracted from the Engelbreth-Holm-Swarm (EHS) mouse sarcoma, with
72    appropriate growth factors (including Wnt3a, epidermal growth factor, Noggin and R-spondin
73    1). The resulting organoids consisted of organ-specific tissue (gastric or intestinal epithelia)
74    that self-organised into spherical three-dimensional (3D) structures with a single epithelial
75    layer and a central lumen (Sato et al., 2009; Barker et al., 2010). Since this initial discovery,
76    organoids have been derived from a large number of different tissue types and from numerous
77    mammalian species using similar ASC isolation and tissue culture techniques.

78    The development of *in vitro* organoid culture systems has transformed biomedical
79    research as they provide a reproducible cell culture system that closely represents the
80    physiology of the host. As the majority of infectious agents enter the body or reside at mucosal
81    surfaces, organoids derived from mucosal sites such as the gastro-intestinal, respiratory and
82    urogenital tracts promise to transform research into host-pathogen interactions as they allow
83    detailed studies of early infection processes that are difficult to address using animal models.

84    Gastrointestinal (GI) disease in small ruminants has significant implications for animal
85    health and welfare as well as substantial economic losses because of decreased production
86    efficiency. In sheep, gastrointestinal nematodes (GIN) have major economic and welfare
87    impacts worldwide, with the principal GIN of sheep including: *Haemonchus contortus*;
88    *Nematodirus battus*; *Teladorsagia circumcincta* and *Trichostrongylus* spp. (including *T.*
89    *colubriformis* and *T. vitrinus*) (Nieuwhof and Bishop, 2005; Roeber et al., 2013). These
90    parasites are transmitted by the faecal-oral route where infective stage larvae develop in either
91    the small intestine or abomasum (which is analogous to the gastric stomach) causing significant
92    mucosal damage associated with host inflammatory immune responses (Stear et al., 2003;
93    Roeber et al., 2013). In addition, sheep are natural reservoirs for enteric zoonotic pathogens of
94    worldwide significance, such as Shiga toxin producing *Escherichia coli* (STEC) and
95    *Salmonella enterica* (Heredia and García, 2018). The obvious challenge with studying
96    interactions between the ovine host and GI pathogens is the lack of accessibility to the site of
97    infection, making detailed studies particularly challenging. With the current lack of
98    physiologically relevant *in vitro* cell culture systems to study ovine-GI pathogen interactions,

99   research has relied heavily on use of sheep infection models, which have led to important
100  insights into host immune responses against pathogens, immune evasion by pathogens and
101  pathogen transmission (Stear et al., 1995; McSorley et al., 2013; Ellis et al., 2014). Despite
102  these successes, animal experiments are often complex, costly and have ethical implications.
103          The use of stem-cell derived GI organoids or "mini-guts" for farmed livestock species,
104  including ruminants, is an exciting recent development that promises to provide a
105  physiologically relevant and host-specific *in vitro* cell culture system to interrogate host-
106  pathogen interactions (Beaumont et al., 2021; Kar et al., 2021). A recent study has
107  demonstrated the feasibility of generating organoids from bovine ileum tissue with the derived
108  organoids expressing genes associated with intestinal epithelia cell types (Hamilton et al.,
109  2018). However, no ruminant gastric organoid model has been previously reported. In this
110  current study, in line with 3Rs principles to reduce and replace the use of animals in
111  experiments, we develop ovine ileum and abomasum organoids as physiologically relevant *in*
112  *vitro* culture systems to investigate ovine GI infection and disease (Figure 1). Using RNA-seq
113  of both tissue and derived organoids we demonstrate that the expression profile of abomasum
114  and ileum organoids are representative of the tissue from which they were derived. In addition,
115  we demonstrate the utility of these *in vitro* organoid systems to study host-pathogen
116  interactions by performing challenge studies with the abomasal parasite *T. circumcincta* and
117  enteric bacteria *Salmonella enterica* serovar Typhimurium.
118
119  **2. Materials and Methods**
120
121  **2.1 Animals**
122  All ovine abomasum and ileum tissues used in this study were derived from 7-8-month old
123  helminth-free Texel cross male lambs (*Ovis aries*).
124
125  **2.2 Isolation of gastric glands and intestinal crypts**
126  Tissues were removed from sheep at post-mortem. Approximately 10 cm$^2$ sections of fundic
127  gastric fold were collected from the abomasum and approximately 10 cm sections of ileal tissue
128  were collected from a region ~ 30 cm distal to the ileocecal junction. Tissues were removed
129  using a sterile scalpel and forceps and placed into sterile ice-cold Hank's buffered saline
130  solution (HBSS) containing 25 µg/ml gentamicin (G1397-10ML; Sigma-Aldrich) and 100
131  U/ml penicillin/streptomycin. To expose the epithelial surfaces, the abomasum was opened
132  along the greater curvature and the ileum opened longitudinally using dissection scissors. The
133  luminal surfaces were rinsed with tap water to remove digesta and then placed onto sterile Petri
134  dishes. The majority of the mucus layer was gently removed using a glass slide, after which
135  the surface mucosal tissue (containing the gastric glands or intestinal crypts) was collected by
136  firm scraping with a fresh glass slide. Mucosal tissue was then transferred to a Falcon tube
137  containing 50 ml of HBSS containing 25 µg/ml gentamicin and 100 U/ml
138  penicillin/streptomycin. Samples were centrifuged at 400 x *g* for 2 min, resulting in a tissue
139  pellet with a mucus layer on top. The supernatant and top forming mucus layer were aspirated
140  and discarded and the tissue was re-suspended in 50 ml of HBSS containing 25 µg/ml
141  gentamicin and 100 U/ml penicillin/streptomycin. This process of centrifugation, aspiration
142  and resuspension was repeated until a mucus layer was no longer visible above the pellet. To
143  release gastric glands and intestinal crypts from tissue, pellets were re-suspended in 25 ml of
144  digestion medium (Dulbecco's Modified Eagle Medium [DMEM] high glucose, (11574486;
145  Gibco) 1 % FBS, 20 µg/ml dispase (4942086001; Roche), 75 U/ml collagenase (C2674; Sigma-
146  Aldrich) 25 µg/ml gentamicin and 100 U/ml penicillin/streptomycin) and incubated
147  horizontally in a shaking incubator at 80 rpm for 40 minutes at 37 °C. Following digestion, the
148  tube was gently shaken to loosen the cells and then left briefly at room temperate to allow large

149 tissue debris to settle. The supernatant was transferred to a sterile 50 ml Falcon tube and
150 gland/crypt integrity within the supernatant was assessed by light microscopy. Samples were
151 then centrifuged at 400 x $g$ for 2 minutes, with the resulting supernatant containing released
152 glands or crypts. The gland/crypt-containing supernatant was washed by centrifugation at 400
153 x $g$ for 2 minutes and the glands/crypts re-suspended in 1-2 ml advanced DMEM/F12 (12634-
154 010; Gibco) containing 1X B27 supplement minus vitamin A (12587-010; Gibco), 25 µg/ml
155 gentamicin and 100 U/ml penicillin/streptomycin.
156
157 **2.4 Organoid culture**
158 Two-hundred to one-thousand gastric glands or intestinal crypts were re-suspended in 100 µl
159 advanced DMEM/F12 medium (containing 1X B27 supplement minus vitamin A, 25 µg/ml
160 gentamicin and 100 U/ml penicillin/streptomycin) and were then added to 150 µl of BD Growth
161 Factor Reduced Matrigel Matrix (356230; BD Biosciences). Fifty microliter droplets were
162 added to consecutive wells of a 24-well tissue culture plate (3524, Corning). Plates were
163 incubated at 37 °C, 5% $CO_2$ for 15-20 minutes to allow the Matrigel to polymerize and then
164 550 µl of pre-warmed complete IntestiCult Growth Medium (mouse) (6005; STEMCELL
165 Technologies) containing 500 nM Y-27632 (10005583; Cambridge Bioscience), 10 µM
166 LY2157299 (15312; Cambridge Bioscience), 10 µM SB202190 (ALX-270-268-M001; Enzo
167 Life Sciences) and gentamicin (50 µg/ml) were added to each well. Plates were incubated at
168 37 °C, 5% $CO_2$ to allow organoids to develop, replacing complete IntestiCult medium every 2-
169 3 days. Organoids were typically cultured for 7-14 days prior to passaging. Phase contrast
170 microscopy was used to image organoids from passage one to passage five, following seven
171 days of *in vitro* growth at each passage.
172
173 **2.5 Organoid passage**
174 IntestiCult media was removed from the cultured organoids and the Matrigel matrix was
175 dissolved by replacement with 1 ml ice-cold advanced DMEM/F12. The re-suspended
176 organoids were transferred to a 15 ml Falcon tube and the total volume of advanced
177 DMEM/F12 was increased to 10 ml. Samples were left on ice for 5 minutes to allow organoids
178 to settle and the supernatant was removed. The organoids were re-suspended in 200 µl
179 advanced DMEM/F12 medium (containing 1X B27 supplement minus vitamin A, 25 µg/ml
180 gentamicin and 100 U/ml penicillin/streptomycin) and then mechanically disrupted by
181 repeatedly pipetting (approximately fifty times) using a 200 µl pipette tip bent at a 90° angle.
182 The number of organoid fragments were counted by light microscopy and samples diluted to
183 200-1000 crypts per 100 µl. One-hundred microliters of fragments were then combined with
184 Matrigel and plated into 24-well tissue culture plates as described in section 2.4. Phase contrast
185 microscopy was used to image organoids from passage one to passage five, following seven
186 days of *in vitro* growth at each passage.
187
188 **2.6 Organoid cryopreservation**
189 IntestiCult media was removed from the cultured organoids and the Matrigel matrix was
190 dissolved by replacement with 1 ml ice-cold advanced DMEM/F12. The re-suspended
191 organoids were transferred to a microcentrifuge tube and pelleted by centrifugation at 290 x $g$
192 for 5 minutes at 4 °C. Following centrifugation, the supernatant was removed and organoid
193 pellets were re-suspended in Cryostor CS10 cryopreservation medium (STEMCELL
194 Technologies) at approximately 500-1000 organoids/ml before being transferred to a cryovial.
195 Cryovials were stored in a cryogenic freezing container for 2 hours at -80 °C and subsequently
196 transferred to -196 °C for long-term storage.
197 Cryopreserved organoids were resuscitated by thawing cryovials in a water bath at 37
198 °C and then rapidly transferring the organoids into a 15 ml Falcon tube containing 8 ml of

199    advanced DMEM/F12 medium (containing 1X B27 supplement minus vitamin A, 25 µg/ml
200    gentamicin and 100 U/ml penicillin/streptomycin). The cryovial was washed with a further 1
201    ml of media and added to the Falcon tube. Samples were pelleted by centrifugation at 290 x g
202    for 5 minutes at 4 °C and then re-suspended in 200 µl of fresh advanced DMEM/F12 medium
203    (containing 1X B27 supplement minus vitamin A, 25 µg/ml gentamicin and 100 U/ml
204    penicillin/streptomycin). Re-suspended organoids were added to Matrigel and cultivated as
205    described in Section 2.4. Organoids were imaged by phase contrast microscopy following
206    seven days of *in vitro* growth prior to cryopreservation and post-cryopreservation.
207
208    **2.7 Total RNA extraction**
209    Total RNA was extracted from gastric and intestinal organoids after multiple serial passages
210    that included passage 0 (P0) through to passage 4 (P4). Ovine gastric and intestinal organoids
211    were prepared as described above; organoids that were formed from animal tissue-derived
212    crypts were designated P0 and these were cultured by serial passage until P4. Each passage
213    was cultured in triplicate wells of a 24-well tissue culture plate and allowed to mature for seven
214    days before collecting for total RNA extraction. For total RNA extraction, IntestiCult media
215    was removed from wells and replaced with 1 ml of ice-cold advanced DMEM/F12. The
216    resulting suspension containing dissolved Matrigel and organoids was transferred to 15 ml
217    sterile Falcon tubes and brought up to 10 ml with ice-cold advanced DMEM/F12. Organoids
218    were gently pelleted by centrifugation at 200 x *g* for 5 min and the supernatant removed.
219    Organoid pellets were re-suspended in 350 µl RLT buffer (Qiagen) containing β-
220    mercaptoethanol, according to manufacturer's guidelines and stored at -70°C. Total RNA was
221    isolated from each sample using a RNeasy mini kit (Qiagen) with the optional on-column
222    DNase digest and total RNA eluted in 30 µl nuclease-free water, according to the manufacturers
223    protocol. Total RNA from each extraction was quantified using a NanoDrop$^{TM}$ One
224    spectrophotometer and integrity analysed using a Bioanalyzer (Agilent) with the RNA 6000
225    Nano kit. Purified total RNA was stored at -70°C until RNA-seq analysis.
226            Total RNA was also extracted from ovine abomasum and ileum tissue harvested at post-
227    mortem from five individual 6-month old helminth-free Texel cross lambs and stored in
228    RNAlater (ThermoFisher). Specifically, samples were taken from the same tissue regions
229    stated above for crypt isolation. For total RNA isolation, approx. 30 mg of tissue was
230    homogenized in 600 µl of RLT buffer containing β-mercaptoethanol using a Precellys® Tissue
231    Homogenizer with CK28 tubes using x3 10s pulses at 5500 rpm with 5 min on ice between
232    each pulse (Bertin Instruments$^{TM}$). Total RNA was isolated and quantified as described
233    previously, except the total RNA was eluted in 50 µl nuclease-free water. Purified total RNA
234    was stored at -70°C until RNA-seq analysis.
235
236    **2.8 RNA-seq Analysis**
237    For each sample, 1 µg of total RNA was used for RNA-seq analysis. All library synthesis and
238    sequencing were conducted at The University of Liverpool, Centre for Genomic Research
239    (CGR). In brief, dual-indexed, strand-specific RNA-seq libraries were constructed from
240    submitted total RNA sample using the NEBNext® Poly(A) mRNA Magnetic Isolation Module
241    (NEB #E7490) and NEBNext Ultra II Directional RNA Library Prep Kit for Illumina (NEB
242    #E7760). A total of 20 libraries were constructed [including: ovine abomasum organoid P0-P4
243    (triplicate pooled wells for each passage); ovine ileum organoid P0-P4 (triplicate pooled wells
244    for each passage); ovine abomasum tissues (n = 5); ovine ileum tissues (n = 5)]. The barcoded
245    individual libraries were pooled and sequenced on a single lane of an Illumina NovaSeq
246    flowcell using S1 chemistry (Paired-end, 2x150 bp sequencing, generating an estimated 650
247    million clusters per lane). Following sequencing adaptors were trimmed using
248    Cutadapt version 1.2.1 (Martin, 2011) and reads were further trimmed using Sickle version

249 1.200 (Joshi and Fass, 2011) with a minimum window quality score of 20. Reads shorter than
250 15 bp after trimming were removed. Sequence reads were checked for quality using FastQC
251 v0.11.7. Reads were pseudo-aligned to the *Ovis aries* transcriptome (Oar_v3.1
252 GCA_000298735.1) using Kallisto v0.46.2 with default settings (Bray et al., 2016) and read
253 abundance calculated as transcripts per million (TPM). Gene expression data was analysed by
254 principal component analysis (PCA) using pcaExplorer version 2.12.0 R/Bioconductor
255 package (Marini and Binder, 2019). Specific genes were also manually retrieved from our
256 transcriptomic dataset and their TPM values $\log_2$ transformed for presenting in heat maps,
257 which were generated using GraphPad Prism software (v8.0).
258
259 **2.9 Immunohistochemistry**
260 Abomasum and ileum organoids were cultivated in Matrigel for 7 days in 8-well chamber slides
261 (354118; Falcon) as described in section 2.4. To make organoids accessible to
262 immunohistochemistry reagents, the culture medium was removed and replaced with ice-cold
263 4% paraformaldehyde. For fixation, samples were kept at 4 °C for 20 minutes to also dissolve
264 the Matrigel and prevent it from re-solidifying. Organoids were washed twice with IF buffer
265 (0.1% Tween20 in PBS) and then permeablised with 0.1% TritonX-100 in PBS for 20 minutes
266 at room temperature. Samples were washed three times with IF buffer and then blocked for 30
267 minutes with 1% BSA in IF buffer at room temperature. Next, primary antibodies diluted in
268 blocking solution were added to the organoids and samples were left overnight at 4 °C. Primary
269 antibodies used included polyclonal rabbit α-Ki67 (ab15580, abcam, used at a 1:500 dilution),
270 polyclonal rabbit α-EPCAM (orb10618, Biorbyt, used at a 1:600 dilution), monoclonal mouse
271 α-villin (sc-58897, Santa Cruz Biotechnology, used at a 1:200 dilution) and monoclonal mouse
272 α-pan cytokeratin (used at a 1:100 dilution). For isotype controls, mouse or rabbit IgG were
273 used in place of the specific primary antibodies and were diluted at 1:100 or 1:500 for mouse
274 and rabbit IgG respectively. The next day, samples were washed three times with IF buffer and
275 then secondary antibodies added (diluted at 1:500 in blocking buffer) and incubated at room
276 temperature for 1 hour. Secondary antibodies used were goat α-mouse Alexa Fluor 488
277 (ab150117, abcam) and goat α-rabbit Alexa Fluor 488 (ab150081, abcam). Phalloidin-iFluor
278 555 reagent (ab176756, abcam, used at a 1:1000 dilution) was also added during the secondary
279 antibody step to label F-actin. Samples were washed three times with IF buffer and then
280 Hoechst 33258 solution diluted 1:200 in IF buffer was added to label nuclei (94403, Sigma-
281 Aldrich). Samples were incubated for a further 5 minutes at room temperature before three
282 washes with IF buffer. Finally, slides were mounted using ProLong Gold antifade mountant
283 (P10144, ThermoFisher Scientific) and imaged by confocal microscopy using a Zeiss LSM
284 710 Inverted Confocal Microscope and Zeiss Zen Black operating software.
285
286 **2.10 Exsheathment of *Teladorsagia circumcincta* third stage larvae (L3)**
287 *T. circumcincta* L3 (Moredun isolate MTci2, CVL) were exsheathed and labelled using
288 modified protocols previously published (Dinh et al., 2014; Bekelaar et al., 2019). Nine
289 milliliters of Earle's balanced salts solution (EBSS) buffer in a 15 ml Falcon tube was preheated
290 in a water bath to 37 °C and $CO_2$-saturated over 1 hour using an incubator tube connected to a
291 $CO_2$ tank. Approximately $5x10^4$ *T. circumcincta* L3 in 1 ml of tap water were added to the
292 $CO_2$-saturated EBSS and the sample continued to be saturated for a further 15 minutes. The
293 Falcon tube was then sealed with Parafilm® M and inverted 6 times before being placed
294 horizontally into an incubator at 37 °C, 5% $CO_2$ for 4 hours. Following incubation, the whole
295 sample was transferred into a 25 cm² vented cap flask and incubated overnight at 37 °C /5%
296 $CO_2$, to allow L3s to continue exsheathing. Exsheathment was validated the following morning
297 by light microscopy. The larvae were then washed 4 times by repeated centrifugation at 330 x
298 *g* for 2 minutes and re-suspension in 50 ml of distilled water (pre-warmed to 37°C). After the

6

299  final wash, the L3 larvae were re-suspended in 1 ml distilled water and transferred to a
300  microcentrifuge tube. Exsheathed L3 (exL3) were fluorescently labelled by the addition of 2
301  µl PKH26 dye (1 mM stock concentration) from the MINI26 PKH26 Red Fluorescent Cell
302  Linker Kit (Sigma-Aldrich) and mixed by pipetting. Parasites were incubated with the dye for
303  15 minutes at room temperature, protected from light. Excess dye was removed by washing the
304  larvae five times with distilled water as described above before finally re-suspending them in
305  1 ml of complete IntestiCult organoid growth medium.
306
307  **2.11 *Teladorsagia circumcincta* L3-organoid co-culture**
308  Abomasum and ileum organoids were cultivated in Matrigel for 7 days in 8-well chamber slides
309  (354118; Falcon) as described in section 2.4. Immediately prior to organoid-*T. circumcincta*
310  co-culture, complete IntestiCult media was removed from the cultured organoids and replaced
311  with 250 µl of fresh pre-warmed complete IntestiCult. Twenty to 50 PKH26 labelled *T.*
312  *circumcincta* exL3 in 50 µl complete IntestiCult media were added to each well of organoids
313  and organoid-larval cultures incubated at 37°C, 5% $CO_2$. Note that organoids were not removed
314  from their Matrigel domes prior to the addition of *T. circumcincta* L3. Upon observation of
315  multiple organoids containing *T. circumcincta* L3 within their lumen (after ~24-48 hours of
316  organoid-*T. circumcincta* co-culture) the samples were fixed with 4% PFA for 30 min,
317  followed by 3 washes with PBS, and stored at 4°C until fluorescence staining. Organoids were
318  permeabilized, blocked and probed with Phalloidin-488 and Hoechst 33258 as described for
319  organoid immunohistochemistry above. Images were captured using a Zeiss LSM 710 Inverted
320  Confocal Microscope and Zeiss Zen Black operating software.
321
322  **2.12 Generation of apical-out organoids**
323  Epithelial polarity was inverted in gastric and intestinal ovine organoids by following a
324  previously published method for reverse polarity in human intestinal organoids (Co et al.,
325  2019). Briefly, gastric and intestinal organoids were grown in Matrigel as described above for
326  7 days. Matrigel domes containing developed organoids were gently dissolved by the addition
327  of 500 µl ice-cold 5 mM EDTA in PBS, taking care not to rupture the organoids. The resulting
328  suspension was transferred to a 15 ml Falcon tube that was subsequently filled with 14 ml of 5
329  mM EDTA in PBS. Samples were placed on a rocker and mixed gently for 1 hour at 4 °C.
330  Organoids were pelleted by centrifugation at 200 x *g* for 3 min at 4 °C and the supernatant was
331  removed. Pellets were re-suspended in complete IntestiCult growth media (containing 500 nM
332  Y-27632, 10 µM LY2157299, 10 µM SB202190 and gentamicin (50 µg/ml), with the addition
333  of 10 % advanced DMEM/F12 medium (containing 1X B27 supplement minus vitamin A, 25
334  µg/ml gentamicin and 100 U/ml penicillin/streptomycin). Re-suspended organoids were
335  transferred to the wells of 8-well glass chamber slides and incubated at 37 °C, 5 % $CO_2$ for a
336  period of 72 hours, prior to being fixed and stained with Phalloidin-iFluor 555 reagent and
337  Hoechst 33258, as described in section 2.9. Confocal imaging was performed as described in
338  section 2.9.
339
340  **2.13 Infection of apical-out organoids with *Salmonella enterica* serovar Typhimurium**
341  The polarity of gastric and intestinal organoids was inverted as described above. *Salmonella*
342  Typhimurium strain ST4/74 was chosen for this experiment as its full genome sequence is
343  available (Richardson et al., 2011) and it has been shown to efficiently invade the ovine ileal
344  mucosa and elicit inflammatory responses in an ovine ligated ileal loop model (Uzzau et al.,
345  2001). To aid visualization of the bacteria in organoids, the strain was electroporated with
346  plasmid pFPV25.1 which carries *gfpmut3A* under the control of the rpsM promoter resulting in
347  the constitutive synthesis of green fluorescent protein (Valdivia and Falkow, 1996). Stability
348  of the plasmid in the absence of antibiotic selection during *Salmonella* infection has been

349 confirmed (Vohra et al., 2019). The bacteria were grown on Luria Bertani (LB) agar
350 supplemented with 100 µg/ml ampicillin at 37 ℃ overnight. Single colonies were transferred
351 to LB broth supplemented with the same antibiotic and grown for 20 hours shaking at 180 rpm
352 at 37 ℃. The liquid cultures were diluted to 3.3 x $10^6$ CFU/ml in complete IntestiCult growth
353 medium, described above, and 300 µl of the dilution was added to half of the wells, which
354 already contained organoids that had already been maintained in conditions for generating
355 apical-out organoids for 72 hours. The other half of the wells acted as negative controls, with
356 organoids being re-suspended in 300 µl of complete IntestiCult growth medium alone (no
357 bacteria). After 30 minutes of incubation another 300 µl of complete IntestiCult growth
358 medium with 200 µg/ml gentamycin was added to kill extracellular bacteria. The slides were
359 incubated at 37 ℃, 5% $CO_2$ for a total of 6 hours. At the end of the incubation period the entire
360 volume of the liquid from each well, including the organoids, were transferred to separate 15ml
361 Falcon tubes (Corning, UK). All centrifugations for organoid collection during washing were
362 done at 200 rpm for 5 minutes. The supernatant was removed and the organoids were washed
363 twice in PBS, and then re-suspended in 4% PFA for 30 minutes for fixation. The organoids
364 were processed for immunohistochemistry as described in section 2.9 and stained with
365 Phalloidin-iFluor 555 reagent, prior to mounting with ProLong Diamond antifade mountant
366 (P36961, ThermoFisher Scientific). Confocal imaging was performed as described in section
367 2.9.
368
369 **3. Results**
370 **3.1 Growth of ovine gastrointestinal organoids *in vitro***
371 Fragmented gastric glands and intestinal crypts isolated from the abomasum fundic fold and
372 the ileum of 7 to 8-month old Texel cross lambs were embedded in Matrigel and grown in
373 complete IntestiCult organoid growth medium. Under identical growth conditions, epithelial
374 stem cells from these two different organ tissues were able to develop into organoids *in vitro*
375 (Figure 2A). By 24 hours, sealed spherical structures containing a central lumen had formed in
376 both the abomasum and ileum organoids. However, while the ileum organoids became
377 branched after 5-7 days of *in vitro* culture, the vast majority of abomasum organoids retained
378 a spherical structure that persisted for the duration of a culture passage (Figure 2A, B).
379 Abomasum and ileum organoids could be serially passaged by removal from Matrigel,
380 fragmentation by pipetting and re-embedding in Matrigel. At each passage, ileum organoids
381 continued to form into branched structures, while the abomasum organoids persistently formed
382 spherical structures. (Figure 2B). Organoids that were cryopreserved in liquid nitrogen after 7
383 days of *in vitro* culture could be thawed and re-cultured, demonstrating the potential to store
384 organoids long-term and to resuscitate when required. Furthermore, we found that the
385 cryopreserved organoids can be resuscitated after at least 18 months of storage in liquid
386 nitrogen. Abomasum and ileum organoids retained their spherical and branched structures,
387 respectively, following resuscitation and 7 days of *in vitro* culture (Figure 2C).
388
389 **3.2 Epithelial cell markers associated with ovine gastric and intestinal organoids**
390 Immunohistochemistry was performed to identify key structural features associated with both
391 abomasum and ileum organoids. Individual Z-stack images of organoids stained with
392 phalloidin to label F-actin clearly demonstrated that the apical surface of the epithelium is
393 present on the interior of the organoid, for both abomasum and ileum organoids, indicated by
394 the presence of a solid F-actin-positive boundary (Figure 3A, 4A). This imaging also confirmed
395 the presence of a hollow lumen within the organoids (Figure 3A, 4A).
396 The proliferation marker Ki67 was detectable in both the abomasum and ileum
397 organoids, indicating that cell division continued to take place after 7 days of *in vitro* culture
398 (Figure 3B, 4B). The epithelial cell markers EpCAM (epithelium cell adherence molecule),

399  villin (epithelium-specific actin-binding protein) and cytokeratin (epithelial cell cytoskeleton
400  filament protein) were each detectable in abomasum and ileum organoids (Figure 3B, 4B),
401  confirming the differentiation of stem cells into epithelium cell-containing organoids. Control
402  samples of organoids probed with mouse and rabbit serum IgG did not label positive for any
403  of the epithelial cell markers, confirming the specificity of the epithelial cell labelling (Figure
404  S1, S2).
405
406  **3.3 Transcriptional analysis of abomasum and ileum organoids and tissue**
407  Gene expression profiles from: ovine ileum organoids (P0 – P4); ovine abomasum organoids
408  (P0 – P4); ovine ileum tissue (n = 5) and ovine abomasum tissue (n = 5) were compared by
409  RNA-seq analysis. The global gene expression profiles of the complete dataset, consisting of
410  20 individual samples, were initially compared by principal component analysis (PCA) (Figure
411  5). The PCA analysis resulted in four statistically significant clusters(with 95% confidence
412  intervals), with each cluster representing a sample type (i.e. ileum organoids; abomasum
413  organoids; ileum tissue; or abomasum tissue). This initial analysis demonstrates that replicate
414  samples collected from either ileum tissue (n = 5) or abomasum tissue (n = 5) group by tissue
415  type showing that the global transcript signature of ileum and abomasum tissue differ. Based
416  on global gene expression profiles, organoids also grouped by the tissue type from which they
417  derived, with ileum and abomasum organoids forming separate statistically significant clusters
418  (95% confidence intervals) in the PCA analysis (Figure 5). Importantly, for both ileum and
419  abomasum organoids, each passage (P0 – P4) is represented in each cluster, showing that there
420  was no global change in the transcriptome profile following serial passage (Figure 5).
421      The expression profiles of the top 40 most variable genes (of genes ranked by inter-
422  sample variation) were compared from ileum and abomasum organoids from serial passages
423  (P0 – P4) and ileum and abomasum tissue derived from five lambs (n = 5) (Figure 6). This
424  analysis broadly identified three categories of genes, including genes with: i) abomasum (tissue
425  and organoid) specific expression; ii) ileum (tissue and organoid) specific expression and iii)
426  ileum and abomasum (tissue only) expression.
427      Based on gene expression profiles, genes that were highly expressed in abomasum
428  tissue and abomasum organoids, but absent in all ileum samples, included genes of known
429  gastric function, such as: *claudin-18*; *gastrokine*; *gastric lysozyme* and *pepsin*. Similarly, ileum
430  specific genes were detected in both ileum tissue and ileum organoid samples, but absent from
431  all abomasum samples included: *galectin*; *lingual antimicrobial peptide*; *guanylin* (a 15 amino
432  acid peptide secreted from goblet cells). Interestingly, genes shared by ileum tissue and
433  abomasum tissue, but largely absent from organoid cultures, were predominantly immune
434  related genes (such as: C-C motif chemokine 5, regakine-1-like and various immunoglobulin
435  chains) and likely reflect the presence of immune cells in ileal and abomasal mucosal tissue
436  samples, which were not represented in ASC derived ileum and abomasum organoids. In
437  summary, based on transcriptional profiles, abomasum and ileum organoids are broadly
438  representative of the tissues they were derived from and appear to be transcriptionally stable
439  over multiple passages.
440
441  **3.4 Expression of cell- and tissue-specific genes in abomasum and ileum organoids and**
442  **tissues**
443  The ovine gastrointestinal transcriptomic database generated here was manually searched for
444  genes that are representative of specific cell and tissue markers. A total of 151 genes were
445  searched in this way and their expression in abomasum and ileum organoids and tissue was
446  presented in heat maps. A number of cell junction markers were consistently expressed in both
447  organoids and tissue, including genes encoding proteins related to tight junctions, gap
448  junctions, adherens junctions and desmosomes (Figure S3).

449     We identified genes associated with particular epithelial cell subpopulations that were
450 consistently expressed in abomasum and ileum organoids across multiple passages (P0-P4), as
451 well as in ileum and abomasum tissue samples from five individual animals. These include
452 numerous markers associated with stem cells, enterocytes, secretory and mucus-producing
453 cells and Paneth cells (Figure 7). In particular, expression of the stem cell marker LGR5 was
454 higher in both abomasum and ileum organoids compared to the respective tissue samples,
455 indicating the presence of a relatively higher stem cell subpopulation in the organoids
456 compared to tissues (Figure 6). Three enterocyte genes associated with ileum tissue were not
457 detected in ileum organoids, namely *ALPI*, *APOA4* and *APOC3* (Figure 7). These enterocyte
458 markers were not detected in abomasum organoids or abomasum tissue from any of the five
459 individual animals. Expression of several genes associated with homeostasis in gastrointestinal
460 cells was conserved between tissue samples and organoids, for both abomasum and ileum
461 samples. This included *HES1*, *ADAM10*, *ADAM17*, *FGF20* and *SHH* (Figure 7).

462     A number of genes associated with specific epithelial cell subpopulations were
463 differentially expressed in ileum and abomasum tissue. For example, the early enterocyte
464 precursor-associated gene *REG3G*, the Paneth cell marker *DEFB1*, the enteroendocrine cell
465 marker *REG4* and the enteroendocrine cell-derived hormone *GCG* were expressed in ileum
466 tissue and not in abomasum tissue (Figure 7). These genes were also expressed in intestinal
467 organoids and not abomasum organoids, indicating the conservation of tissue-specific
468 differences in the cell subpopulations of the two different types of organoids.

469     Various genes were found to be specific for the abomasum, being expressed in both
470 abomasal tissue and abomasum organoids but not in ileal tissue or ileum organoids. These
471 included *PGA5, CCKBR* and *CBLIF (GIF)* (Figure 8). We also found that some genes
472 specifically expressed in abomasal tissue were not expressed in abomasum organoids,
473 including *SLC5A5, DUOX2, MCT9, PGC, ATP4A, AQP4,* and *HDC* (Figure 8).

474     The expression of immune-related genes, including toll-like receptors (TLRs), c-type
475 lectin receptors (CLRs), chemokines, cytokines and antimicrobials were examined in
476 abomasum and ileum tissue and organoids. The TLRs - *TLR3*, *TLR5* and *TLR6*, and CLR
477 *Dectin-1* were expressed in abomasum and ileum organoids and their respective tissues (Figure
478 S4). A number of chemokines were expressed in abomasum organoids and abomasal tissue,
479 including *CXCL16*, *CCL20*, *CCL24* and *ACKR3*. Interestingly, the chemokine *CCL17* was up-
480 regulated in abomasum and ileum organoids compared to the respective tissue samples (Figure
481 S4). The expression of cytokine associated genes *IL18BP*, *IL27RA*, *IL4I1*, *IL13RA1* and
482 *IFNGR1* was detected in abomasum and ileum organoids (Figure S4). Of note, the
483 antimicrobial gene SBD2 was found to be highly expressed in ileum and ileal tissue, but was
484 not expressed in either abomasum organoids nor abomasal tissue (Figure 6, Figure S4).

485

**3.5 Organoid co-culture with the helminth *Teladorsagia circumcincta***
487 In order to use gastrointestinal organoids to study host-pathogen interactions *in vitro*, it is
488 important to be able to challenge organoids with the pathogen-of-interest. Here, we co-cultured
489 abomasum and ileum organoids with larvae of the important ruminant helminth parasite *T.
490 circumcincta*. Infective, third stage larvae (L3) were ex-sheathed *in vitro* and labelled with the
491 lipophilic dye PKH26. Labelled larvae were added directly to the well of a 24-well tissue
492 culture plate containing abomasum or ileum organoids embedded in Matrigel and complete
493 IntestiCult growth media. A number of *T. circumcincta* L3 penetrated the Matrigel, of which
494 approximately 50% subsequently burrowed into central lumen of the organoids by 24 hours
495 post-incubation, with some individual L3 invading the organoids as early as 2 hours. This
496 indicated that it was possible to infect the organoids with the parasite in the correct orientation
497 (i.e. with the parasite residing at the luminal surface of the organoid) without having to
498 mechanically disrupt the organoids to allow access to the central lumen. *T. circumcincta* L3

499   were equally effective at infecting both abomasum and ileum organoids and motile larvae were
500   still present after 14 days of co-culture. While we mainly observed abomasum organoids
501   containing single larvae (Figure 9A), we found multiple larvae residing in the lumen of the
502   larger ileum organoids (Figure 9B). Z-stack analysis on fixed samples showed worms were
503   present within the lumen of the organoids and demonstrated L3 larvae burrowing directly
504   through the epithelium of abomasum and ileum organoids to access the central lumen (Figure
505   9C).
506
507   **3.6 Generation of apical-out organoids and infection with *Salmonella typhimurium***
508   It is necessary to expose the apical surface of the organoid epithelia in order to have a working
509   co-culture system for some pathogens. A recently published protocol (Co et al., 2019)
510   described a method to invert the basal-out orientation of the abomasum and intestinal
511   organoids. When the organoids were removed from Matrigel and incubated in 5 mM EDTA
512   for 1 hour, the polarity of both the abomasum and intestinal organoids was reversed following
513   72 hours' incubation in complete IntestiCult growth medium. F-actin staining of fixed organoid
514   samples clearly highlighted the apical surface of the epithelium, which is initially internally
515   located in basal-out abomasum and ileum organoids; however, after removing the extra cellular
516   matrix from the organoids, the apical surface became positioned on the exterior surface of the
517   organoids, with a microvilli brush edge apparent by confocal microscopy (Figure 10A, B).
518
519   To demonstrate the utility of apical-out ovine gastric and intestinal organoids as an *in vitro*
520   model for host-pathogen interactions, the apical-out organoids were exposed to the bacterial
521   pathogen *Salmonella enterica* serovar Typhimurium, which is known to invade the epithelium
522   via the apical surface (Finlay and Falkow, 1990). After 6 hours of organoid-bacteria co-culture
523   freely suspended in complete IntestiCult growth medium, GFP-expressing *S.* Typhimurium
524   were identifiable attached to the apical surface and within epithelial cells of the organoids by
525   confocal microscopy. Although *S.* Typhimurium is an intestinal pathogen, here we observed
526   GFP-expressing bacteria attached to both abomasum and ileum apical-out organoids (Figure
527   10C).
528
529   **4. Discussion**
530   Ruminants are key food-producing animals worldwide, providing a nutrient source to billions
531   of people. Furthermore, dependency upon ruminants as a food source continues to increase in
532   order to meet growing global dietary requirements. Gastrointestinal disease in ruminants is a
533   major concern and accounts for significant economic losses and reduction in production
534   efficiency. It is therefore important that ruminant health and welfare is improved through
535   prevention and control of disease in order to meet ethical, economic and nutrient demands
536   (Sargison, 2020).
537         An obvious challenge with studying gastrointestinal host-pathogen interactions *in vivo*
538   is the internal nature of infections and the physical barriers associated with directly observing
539   them. Therefore, a useful advancement for studying such infections is the development of a
540   physiologically relevant *in vitro* model systems that allows experimental interrogation of host
541   and pathogen interactions in fine detail. Stem cell-derived organoids have become a prominent
542   feature of modern cell and tissue biology in recent years, representing *in vitro* cell cultures that
543   retain structural and functional properties of the *in vivo* organ/tissue they represent (Clevers,
544   2016). To date, organoid cultivation has been achieved for numerous and diverse organs and
545   tissues from different host species. In particular, organoids derived from gastrointestinal tissue
546   have been generated for numerous livestock species, including cattle (Hamilton et al., 2018;
547   Beaumont et al., 2021). However, the vast majority of these have been organoids representing
548   the intestinal tract. Here, we demonstrated the ability to cultivate organoids from gastric and

549  intestinal tissues of a small ruminant host and, to our knowledge, this is the first demonstration
550  of organoids representing the gastric system of a ruminant.

551  Following the same protocol and using the same *in vitro* culture conditions, we report
552  the ability to cultivate tissue-specific gastric and intestinal organoids from sheep. By comparing
553  gene expression profiles between tissue and organoids, we found that when grown in identical
554  conditions *in vitro*, stem cells from gastric glands developed into organoids that retained key
555  characteristics associated with abomasum tissue. Stem cells from ileal crypts, on the other
556  hand, developed into organoids which conserved important gene expression profiles associated
557  with the ileum.

558  Ruminants, including cattle, sheep and goats are polygastric, in that they have a four-
559  chambered gastric system. The fourth chamber, the abomasum, is most closely akin to the
560  stomach of monogastric animals. An important differentiating characteristic between
561  abomasum and ileum tissue is the expression of the digestive stomach enzyme pepsinogen in
562  the abomasum (Mostofa et al., 1990). Another digestive protease associated with the
563  abomasum in ruminants is lysozyme, which is highly expressed in this compartment (Stevens
564  and Hume, 1998). Importantly, we found that both pepsinogen and lysozyme are expressed in
565  abomasum organoids and not in ileum organoids. We also found evidence of parietal cells
566  specifically present in abomasum organoids and not ileum organoids. This was indicated by
567  the detection of *CCKBR* mRNA only in abomasum organoids and tissue following
568  transcriptomic analysis. *CCKBR* is a cholecystokinin receptor expressed in the gastric and
569  central nervous systems and more specifically it is associated with parietal cells in the stomach
570  (Kulaksiz et al., 2000; Schmitz et al., 2001; Engevik et al., 2019). Conversely, we also
571  identified genes whose expression was specific to ileum tissue that were also expressed in
572  ileum organoids and not in abomasum organoids. For example, *REG4*, a marker of
573  enteroendocrine cells (specifically enterochromaffin cells) in intestinal epithelia (Gehart et al.,
574  2019) and *SBD2*, an antimicrobial sheep beta-defensin associated with the mucosal surface of
575  small intestinal crypts (Meyerholz et al., 2004) were found to be specifically and abundantly
576  expressed in ileum tissue and organoids and not abomasum. Collectively, these key differences
577  in gene expression indicates that the two different types of organoid are tissue-specific and
578  representative of the tissue from which the stem cells are derived. We also found that a number
579  of genes used in previous studies as gastrointestinal epithelial markers (Hamilton et al., 2018)
580  were not detected in our transcriptomic analysis of ileal or abomasal tissue from five individual
581  animals, suggesting these genes are not reliable markers of gastrointestinal epithelia in sheep.

582  A necessary feature of an organoid cell line is the conservation of gene expression
583  profiles across multiple passages. Transcriptomic analysis of abomasum and ileum organoid
584  samples collected across five consecutive passages revealed that gene expression profiles were
585  consistent. Further analysis of the expression of specific cell markers indicated that the
586  diversity of epithelial cell types was also maintained across multiple passages. That the
587  different organoid types maintain their tissue specificity and cell diversity, as well as the ability
588  to cryopreserve them makes them a robust model that will ensure reproducibility across
589  experiments, as well as reducing the reliance on deriving material from animals and thereby
590  reducing the number of animals used in associated research.

591  To demonstrate the effectiveness of ovine gastric and intestinal organoids for modelling
592  pathogen infections *in vitro*, we exposed abomasum and ileum organoids to different pathogens
593  and showed they could invade them. It has been recognized that gastrointestinal organoids
594  could represent useful *in vitro* models for studying helminth infections (Duque-Correa et al.,
595  2020). However, to-date this has been limited to applying worm excretory and secretory
596  products to organoids, or growing organoids from helminth-infected mice, as opposed to live
597  host-parasite co-cultures (Eichenberger et al., 2018a, 2018b; Nusse et al., 2018; Luo et al.,
598  2019; Duque-Correa et al., 2020). Here, we applied a very simple method of adding ex-

599  sheathed *T. circumcincta* L3 directly to the growth media of organoids that were embedded in
600  Matrigel. We found that after 24 hours, worms had burrowed through the Matrigel dome and
601  into the lumen of individual organoids. We were also able to capture direct *T. circumcincta*
602  invasion through the epithelium in both abomasum and ileum organoids. Furthermore, motile
603  worms were observed at least 14 days following organoid invasion, demonstrating the potential
604  to prolong parasite survival *in vitro* and to perform more long-term studies on the parasite
605  compared to worms cultured under previous *in vitro* methods (*pers comms*).

606      Gastrointestinal pathogens that invade the epithelial mucosa commonly interact with
607  the apical surface of epithelial cells. However, the innate polarity of mammalian
608  gastrointestinal organoids grown in Matrigel is with the apical surface on the inside of the
609  organoid. Various approaches have previously been used to expose pathogens to the apical
610  surface of the epithelium, including microinjection directly into the lumen of the organoid,
611  fragmentation of organoids and open-format 2D monolayers. A recent publication also
612  demonstrated the ability to reverse the polarity of human ileum organoids by the removal of
613  Matrigel and extracellular matrix proteins (Co et al., 2019). This has since been replicated in
614  porcine ileum organoids (Beaumont et al., 2021) and here, we showed that ruminant ileum
615  organoids can also have the polarity reversed following the same method. We also
616  demonstrated that the polarity of gastric organoids can be reversed to an apical-out
617  conformation. The ability to expose the apical surface of gastric and intestinal organoids to the
618  culture supernatant facilitates direct interaction of the organoids with microbes, as we showed
619  here by infecting apical-out organoids with *S*. Typhimurium. Since this method does not require
620  the use of specialist equipment to administer pathogens into a central organoid lumen, this
621  makes modelling host-pathogen infections *in vitro* significantly more practical.

622      In summary, the results from this study demonstrate the ability to isolate stem cells
623  from gastric glands and crypts of the sheep abomasum and intestine, respectively and show
624  that they differentiate into tissue-specific organoids when grown under identical conditions.
625  The robustness of both gastric and intestinal organoids from sheep was demonstrated by
626  showing that tissue-specific gene expression is maintained across multiple passages. Finally,
627  both gastric and intestinal sheep organoids can be invaded by important bacterial and parasitic
628  pathogens and they therefore represent a useful tool for modelling host-pathogen interactions.

629

**5. Conflict of Interest**

631  The authors declare that the research was conducted in the absence of any commercial or
632  financial relationships that could be construed as a potential conflict of interest.

633

**6. Author Contributions**

635  DS, DRGP, EAI and TMcN conceived the study. All authors designed the research. DS, DRGP,
636  AB, KAH, MF, AFC and CC performed research. DS, DRGP and STGB analysed data. DS
637  and DRGP wrote the paper with contributions from all authors. All authors read and approved
638  the final manuscript.

639

**7. Data availability statement**

641  The datasets generated and analysed during the current study are fully compliant with the
642  MINISEQE guidelines and are deposited in the publicly accessible NCBI Sequence Read
643  Archive (SRA) Database under the project accession number PRJNA736945.

644

649 Environment Science and Analytical Services (RESAS). KAH is supported by an Industrial
650 Partnership PhD studentship funded by the University of Glasgow, Moredun Foundation and
651 Pentlands Science Park, UK. MPS and CCU acknowledge funding from the Biotechnology &
652 Biological Sciences Research Council via the Institute Strategic Programme on Control of
653 Infectious Diseases (BB/P013740/1) and its constituent project BBS/E/D/20002173.
654

662

663 **10. References**
664 Barker, N., Huch, M., Kujala, P., van de Wetering, M., Snippert, H. J., van Es, J. H., et al.
665     (2010). Lgr5(+ve) stem cells drive self-renewal in the stomach and build long-lived
666     gastric units in vitro. *Cell Stem Cell* 6, 25–36. doi:10.1016/j.stem.2009.11.013.

667 Barker, N., van Es, J. H., Kuipers, J., Kujala, P., van den Born, M., Cozijnsen, M., et al.
668     (2007). Identification of stem cells in small intestine and colon by marker gene Lgr5.
669     *Nature* 449, 1003–1007. doi:10.1038/nature06196.

670 Beaumont, M., Blanc, F., Cherbuy, C., Egidy, G., Giuffra, E., Lacroix-Lamandé, S., et al.
671     (2021). Intestinal organoids in farm animals. *Veterinary Research* 52, 33.
672     doi:10.1186/s13567-021-00909-x.

673 Bekelaar, K., Waghorn, T., Tavendale, M., McKenzie, C., and Leathwick, D. (2019).
674     Abomasal nematode species differ in their in vitro response to exsheathment triggers.
675     *Parasitol Res* 118, 707–710. doi:10.1007/s00436-018-6183-1.

676 Bray, N. L., Pimentel, H., Melsted, P., and Pachter, L. (2016). Near-optimal probabilistic
677     RNA-seq quantification. *Nature Biotechnology* 34, 525–527. doi:10.1038/nbt.3519.

678 Clevers, H. (2016). Modeling Development and Disease with Organoids. *Cell* 165, 1586–
679     1597. doi:10.1016/j.cell.2016.05.082.

680 Co, J. Y., Margalef-Català, M., Li, X., Mah, A. T., Kuo, C. J., Monack, D. M., et al. (2019).
681     Controlling Epithelial Polarity: A Human Enteroid Model for Host-Pathogen
682     Interactions. *Cell Reports* 26, 2509-2520.e4. doi:10.1016/j.celrep.2019.01.108.

683 Dinh, P. T. Y., Knoblauch, M., and Elling, A. A. (2014). Nondestructive Imaging of Plant-
684     Parasitic Nematode Development and Host Response to Nematode Pathogenesis.
685     *Phytopathology* 104, 497–506. doi:10.1094/PHYTO-08-13-0240-R.

686 Duque-Correa, M. A., Maizels, R. M., Grencis, R. K., and Berriman, M. (2020). Organoids –
687     New Models for Host–Helminth Interactions. *Trends in Parasitology* 36, 170–181.
688     doi:10.1016/j.pt.2019.10.013.

689 Eichenberger, R. M., Ryan, S., Jones, L., Buitrago, G., Polster, R., Montes de Oca, M., et al.
690     (2018a). Hookworm Secreted Extracellular Vesicles Interact With Host Cells and

14

691           Prevent Inducible Colitis in Mice. *Front. Immunol.* 9.
692           doi:10.3389/fimmu.2018.00850.

693    Eichenberger, R. M., Talukder, M. H., Field, M. A., Wangchuk, P., Giacomin, P., Loukas, A.,
694           et al. (2018b). Characterization of Trichuris muris secreted proteins and extracellular
695           vesicles provides new insights into host–parasite communication. *Journal of*
696           *Extracellular Vesicles* 7, 1428004. doi:10.1080/20013078.2018.1428004.

697    Ellis, S., Matthews, J. B., Shaw, D. J., Paterson, S., McWilliam, H. E. G., Inglis, N. F., et al.
698           (2014). Ovine IgA-reactive proteins from Teladorsagia circumcincta infective larvae.
699           *Int J Parasitol* 44, 743–750. doi:10.1016/j.ijpara.2014.05.007.

700    Engevik, A. C., Kaji, I., and Goldenring, J. R. (2019). The Physiology of the Gastric Parietal
701           Cell. *Physiological Reviews* 100, 573–602. doi:10.1152/physrev.00016.2019.

702    Finlay, B. B., and Falkow, S. (1990). Salmonella Interactions with Polarized Human
703           Intestinal Caco-2 Epithelial Cells. *The Journal of Infectious Diseases* 162, 1096–
704           1106. doi:10.1093/infdis/162.5.1096.

705    Gehart, H., van Es, J. H., Hamer, K., Beumer, J., Kretzschmar, K., Dekkers, J. F., et al.
706           (2019). Identification of Enteroendocrine Regulators by Real-Time Single-Cell
707           Differentiation Mapping. *Cell* 176, 1158-1173.e16. doi:10.1016/j.cell.2018.12.029.

708    Hamilton, C. A., Young, R., Jayaraman, S., Sehgal, A., Paxton, E., Thomson, S., et al.
709           (2018). Development of in vitro enteroids derived from bovine small intestinal crypts.
710           *Veterinary Research* 49, 54. doi:10.1186/s13567-018-0547-5.

711    Heredia, N., and García, S. (2018). Animals as sources of food-borne pathogens: A review.
712           *Anim Nutr* 4, 250–255. doi:10.1016/j.aninu.2018.04.006.

713    Joshi, N. A., and Fass, J. N. (2011). Sickle: A sliding-window, adaptive, quality-based
714           trimming tool for FastQ files (Version 1.33). Available at:
715           https://github.com/najoshi/sickle.

716    Kar, S. K., Wells, J. M., Ellen, E. D., te Pas, M. F. W., Madsen, O., Groenen, M. A. M., et al.
717           (2021). Organoids: a promising new in vitro platform in livestock and veterinary
718           research. *Veterinary Research* 52, 43. doi:10.1186/s13567-021-00904-2.

719    Kulaksiz, H., Arnold, R., Göke, B., Maronde, E., Meyer, M., Fahrenholz, F., et al. (2000).
720           Expression and cell-specific localization of the cholecystokinin B/gastrin receptor in
721           the human stomach. *Cell Tissue Res* 299, 289–298.

722    Luo, X.-C., Chen, Z.-H., Xue, J.-B., Zhao, D.-X., Lu, C., Li, Y.-H., et al. (2019). Infection by
723           the parasitic helminth *Trichinella spiralis* activates a Tas2r-mediated signaling
724           pathway in intestinal tuft cells. *Proc Natl Acad Sci USA* 116, 5564–5569.
725           doi:10.1073/pnas.1812901116.

726    Marini, F., and Binder, H. (2019). pcaExplorer: an R/Bioconductor package for interacting
727           with RNA-seq principal components. *BMC Bioinformatics* 20, 331.
728           doi:10.1186/s12859-019-2879-1.

729    Martin, M. (2011). Cutadapt removes adapter sequences from high-throughput sequencing
730            reads. *EMBnet.journal* 17, 10–12. doi:10.14806/ej.17.1.200.

731    McSorley, H. J., Hewitson, J. P., and Maizels, R. M. (2013). Immunomodulation by helminth
732            parasites: defining mechanisms and mediators. *Int J Parasitol* 43, 301–310.
733            doi:10.1016/j.ijpara.2012.11.011.

734    Meyerholz, D. K., Gallup, J. M., Grubor, B. M., Evans, R. B., Tack, B. F., McCray Jr, P. B.,
735            et al. (2004). Developmental expression and distribution of sheep β-defensin-2.
736            *Developmental & Comparative Immunology* 28, 171–178. doi:10.1016/S0145-
737            305X(03)00105-8.

738    Mostofa, M., McKELLAR, Q. A., and Eckersall, P. D. (1990). Comparison of pepsinogen
739            forms in cattle, sheep and goats. *Research in Veterinary Science* 48, 33–37.
740            doi:10.1016/S0034-5288(18)31505-4.

741    Nieuwhof, G. J., and Bishop, S. C. (2005). Costs of the major endemic diseases of sheep in
742            Great Britain and the potential benefits of reduction in disease impact. *Animal Science*
743            81, 23–29. doi:10.1079/ASC41010023.

744    Nusse, Y. M., Savage, A. K., Marangoni, P., Rosendahl-Huber, A. K. M., Landman, T. A., de
745            Sauvage, F. J., et al. (2018). Parasitic helminths induce fetal-like reversion in the
746            intestinal stem cell niche. *Nature* 559, 109–113. doi:10.1038/s41586-018-0257-1.

747    Richardson, E. J., Limaye, B., Inamdar, H., Datta, A., Manjari, K. S., Pullinger, G. D., et al.
748            (2011). Genome Sequences of Salmonella enterica Serovar Typhimurium,
749            Choleraesuis, Dublin, and Gallinarum Strains of Well- Defined Virulence in Food-
750            Producing Animals. *Journal of Bacteriology* 193, 3162–3163. doi:10.1128/JB.00394-
751            11.

752    Roeber, F., Jex, A. R., and Gasser, R. B. (2013). Impact of gastrointestinal parasitic
753            nematodes of sheep, and the role of advanced molecular tools for exploring
754            epidemiology and drug resistance - an Australian perspective. *Parasites & Vectors* 6,
755            153. doi:10.1186/1756-3305-6-153.

756    Sargison, N. D. (2020). The critical importance of planned small ruminant livestock health
757            and production in addressing global challenges surrounding food production and
758            poverty alleviation. *New Zealand Veterinary Journal* 68, 136–144.
759            doi:10.1080/00480169.2020.1719373.

760    Sato, T., Vries, R. G., Snippert, H. J., van de Wetering, M., Barker, N., Stange, D. E., et al.
761            (2009). Single Lgr5 stem cells build crypt-villus structures in vitro without a
762            mesenchymal niche. *Nature* 459, 262–265. doi:10.1038/nature07935.

763    Schmitz, F., Göke, M. N., Otte, J.-M., Schrader, H., Reimann, B., Kruse, M.-L., et al. (2001).
764            Cellular expression of CCK-A and CCK-B/gastrin receptors in human gastric mucosa.
765            *Regulatory Peptides* 102, 101–110. doi:10.1016/S0167-0115(01)00307-X.

766    Stear, M. J., Bishop, S. C., Doligalska, M., Duncan, J. L., Holmes, P. H., Irvine, J., et al.
767            (1995). Regulation of egg production, worm burden, worm length and worm

768   fecundity by host responses in sheep infected with Ostertagia circumcincta. *Parasite*
769   *Immunol* 17, 643–652. doi:10.1111/j.1365-3024.1995.tb01010.x.

770   Stear, M. J., Bishop, S. C., Henderson, N. G., and Scott, I. (2003). A key mechanism of
771   pathogenesis in sheep infected with the nematode Teladorsagia circumcincta. *Anim*
772   *Health Res Rev* 4, 45–52. doi:10.1079/ahrr200351.

773   Stevens, C. E., and Hume, I. D. (1998). Contributions of Microbes in Vertebrate
774   Gastrointestinal Tract to Production and Conservation of Nutrients. *Physiological*
775   *Reviews* 78, 393–427. doi:10.1152/physrev.1998.78.2.393.

776   Uzzau, S., Leori, G. S., Petruzzi, V., Watson, P. R., Schianchi, G., Bacciu, D., et al. (2001).
777   Salmonella enterica Serovar-Host Specificity Does Not Correlate with the Magnitude
778   of Intestinal Invasion in Sheep. *Infection and Immunity* 69, 3092–3099.
779   doi:10.1128/IAI.69.5.3092-3099.2001.

780   Valdivia, R. H., and Falkow, S. (1996). Bacterial genetics by flow cytometry: rapid isolation
781   of Salmonella typhimurium acid-inducible promoters by differential fluorescence
782   induction. *Molecular Microbiology* 22, 367–378. doi:10.1046/j.1365-
783   2958.1996.00120.x.

784   Vohra, P., Vrettou, C., Hope, J. C., Hopkins, J., and Stevens, M. P. (2019). Nature and
785   consequences of interactions between Salmonella enterica serovar Dublin and host
786   cells in cattle. *Veterinary Research* 50, 99. doi:10.1186/s13567-019-0720-5.

787   Xiao, S., and Zhou, L. (2020). Gastric Stem Cells: Physiological and Pathological
788   Perspectives. *Front. Cell Dev. Biol.* 8. doi:10.3389/fcell.2020.571536.

789
790   **11. Figure Legends**
791
792   **Figure 1.** A schematic of the development of ovine gastric and intestinal organoids for studying
793   host-pathogen interactions. Stem cells isolated from sheep ileum crypts and abomasum gastric
794   glands can be cultivated into tissue-specific organoids when grown in a three-dimensional
795   culture system. Gastric and intestinal organoids can be co-cultured with pathogens to model
796   host-parasite interactions in physiologically and biologically-relevant *in vitro* culture systems.
797   Created with BioRender.com.
798
799   **Figure 2.** *In vitro* growth of ovine abomasum and ileum organoids. (A) Representative images
800   of abomasum and ileum organoids grown over 14 days in the same culture conditions. (B)
801   Representative images showing the growth and development of mature abomasum and ileum
802   organoids across multiple consecutive passages (P1 - P5). (C) Representative images of
803   abomasum and ileum organoids grown for seven days, both pre-cryopreservation and after
804   resuscitation. Scale bars = 10 µm.
805
806   **Figure 3.** Characterisation of ovine abomasum organoids by immunofluorescence confocal
807   microscopy. (A) Representative Z-stack images of an individual abomasum organoid with a
808   closed luminal space and an internal F-actin-expressing brush border. Red = F-actin and blue
809   = Hoechst (nuclei). (B) Representative images of abomasum organoids probed for either the
810   cell proliferation marker Ki67, or the epithelial cell markers EpCAM, villin and pan-
811   cytokeratin (all green). F-actin (red) and Hoechst (blue). Scale bars = 10 µm.

17

812

813 **Figure 4.** Characterisation of ovine ileum organoids by immunofluorescence confocal
814 microscopy. (A) Representative Z-stack images of part of an individual branched ileum
815 organoid with a closed luminal space and an internal F-actin-expressing brush border. Red =
816 F-actin and blue = Hoechst (nuclei). (B) Representative images of abomasum organoids probed
817 for either the cell proliferation marker Ki67, or the epithelial cell markers EpCAM, villin and
818 pan-cytokeratin (all green). F-actin (red) and Hoechst (blue). Scale bars = 10 µm.

819

820 **Figure 5.** Principal component analysis (PCA) of RNA-seq expression of the top 500 most
821 variant genes (of genes ranked by inter-sample variance) in ovine abomasum and ileum
822 organoid and tissue samples. Sample type is indicated in the key and includes: abomasum
823 organoid (red); abomasum tissue (green); ileum organoid (blue); ileum tissue (purple). Ellipses
824 indicates 95% confidence intervals for each cluster.

825

826 **Figure 6.** Heat map showing expression level of top 40 most variant genes (of genes ranked
827 by inter-sample variance) from ileum (ile) and abomasum (abo) organoids from serial passages
828 (P0 – P4) and ileum (ile) and abomasum (abo) tissue derived from five lambs (T1 – T5).
829 Colours indicate level of expression from low (blue) to high (red). The dendrograms indicate
830 similarity between samples. Details of genes included in the heat map, including ENSOART
831 sequence identifiers, are shown in Supplemental File 1.

832

833 **Figure 7.** Heat map showing the expression of genes associated with gastrointestinal epithelia
834 in abomasum and ileum tissue and organoids. RNA-seq analysis was performed to compare
835 gene expression in abomasal and ileal tissue derived from five lambs and abomasum and ileum
836 organoids across multiple passages. Squares from left to right under "abomasum tissue" and
837 "ileum tissue" represent lambs T1-T5. Squares from left to right under abomasum organoids
838 and ileum organoids represent passages P0-P4. Scale = $\log_2$ transcripts per million reads. Ee:
839 enteroendocrine. Details of genes included in the heat map, including ENSOART sequence
840 identifiers, are shown in Supplemental File 2.

841

842 **Figure 8.** Heat map showing the expression of genes associated with gastric epithelia in
843 abomasum and ileum tissue and organoids. RNA-seq analysis was performed to compare gene
844 expression in abomasal and ileal tissue derived from five lambs and abomasum and ileum
845 organoids across multiple passages. Squares from left to right under "abomasum tissue" and
846 "ileum tissue" represent lambs T1-T5. Squares from left to right under abomasum organoids
847 and ileum organoids represent passages P0-P4. Scale = $\log_2$ transcripts per million reads.
848 Details of genes included in the heat map, including ENSOART sequence identifiers, are
849 shown in Supplemental File 2.

850

851 **Figure 9.** Ovine gastric and intestinal organoids modelling a helminth infection. (A)
852 Representative images of ovine abomasum and ileum organoids challenged with the helminth
853 parasite *Teladorsagia circumcincta*. Following 24 hours of co-culture, L3 stage T.
854 circumcincta (red) are visible within the lumen of abomasum and ileum organoids. (B)
855 Representative images of individual ileum organoids presenting an enlarged lumen containing
856 multiple worms (red). (C) Representative Z-stack images showing L3 stage *T. circumcincta*
857 (red) migrating through the epithelial layer in abomasum and ileum organoids. F-actin (green)
858 and Hoescht (blue). Scale bars = 10 µm.

859

860 **Figure 10.** Reverse polarisation of ovine gastric and intestinal organoids for modelling host-
861 pathogen interactions across the apical surface. Basal-out and apical-out abomasum (A) and

18

862 ileum (B) organoids imaged by differential interference contrast (top) and confocal
863 immunofluorescence microscopy (bottom). White arrows indicate the F-actin-expressing brush
864 border associated with the apical surface of the epithelia. Yellow arrow in the inset panel
865 indicates microvilli at the externally located brush border in apical-out organoids. (C) Cross
866 sections of apical-out abomasum and ileum organoids imaged by confocal microscopy. GFP-
867 expressing *Salmonella enterica* Typhimrium (green), indicated by white arrows, are detectable
868 on the surface of and within epithelial cells. F-actin (red) and Hoechst (blue). Scale bars = 10
869 µm.

870

871 **Supplemental Figure 1.** Negative controls for immunofluorescence antibody labelling in
872 abomasum organoids. Representative confocal microscopy images of abomasum organoids
873 probed with non-specific host IgG followed by indirect Alexa Fluor® 488-conjugated
874 secondary antibody labelling. Marker name in green brackets indicates the antibody labelling
875 control each organoid image represents. Scale bars = 10 µm.

876

877 **Supplemental Figure 2.** Negative controls for immunofluorescence antibody labelling in
878 intestinal organoids. Representative confocal microscopy images of ileum organoids probed
879 with non-specific host IgG followed by indirect Alexa Fluor® 488-conjugated secondary
880 antibody labelling. Marker name in green brackets indicates the antibody labelling control each
881 organoid image represents. Hoecsht, blue. Scale bars = 10 µm.

882

883 **Supplemental Figure 3.** Heat map showing the expression of cell junction-related genes in
884 abomasum and ileum tissue and organoids. RNA-seq analysis was performed to compare gene
885 expression in abomasal and ileal tissue derived from five lambs and abomasum and ileum
886 organoids across multiple passages. Squares from left to right under "abomasum tissue" and
887 "ileum tissue" represent lambs T1-T5. Squares from left to right under abomasum organoids
888 and ileum organoids represent passages P0-P4. Scale = $\log_2$ transcripts per million reads.
889 Details of genes included in the heat map, including ENSOART sequence identifiers, are
890 shown in Supplemental File 2.

891

892 **Supplemental Figure 4.** Heat map showing the detection of immune-related gene expression
893 in abomasum and ileum tissue and organoids. RNA-seq analysis was performed to compare
894 gene expression in abomasal and ileal tissue derived from five lambs and abomasum and ileum
895 organoids across multiple passages. Squares from left to right under "abomasum tissue" and
896 "ileum tissue" represent lambs T1-T5. Squares from left to right under abomasum organoids
897 and ileum organoids represent passages P0-P4. Scale = $\log_2$ transcripts per million reads. TLRs:
898 toll-like receptors. CLRs: C-type lectin receptors. Details of genes included in the heat map,
899 including ENSOART sequence identifiers, are shown in Supplemental File 2.

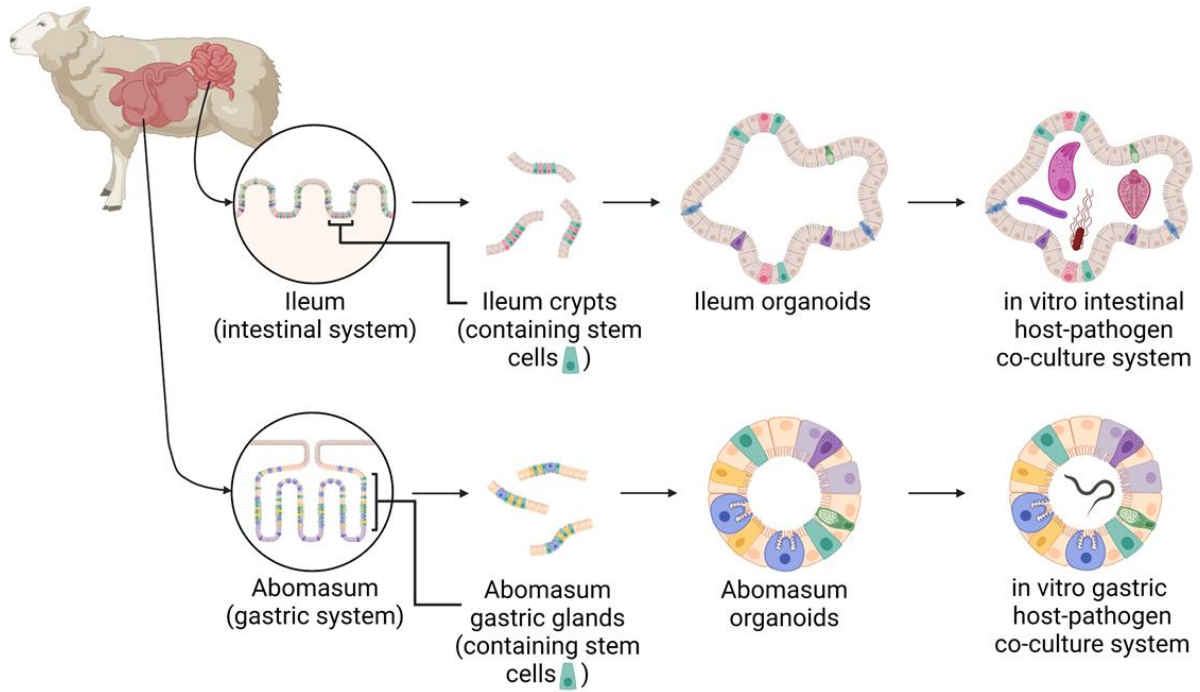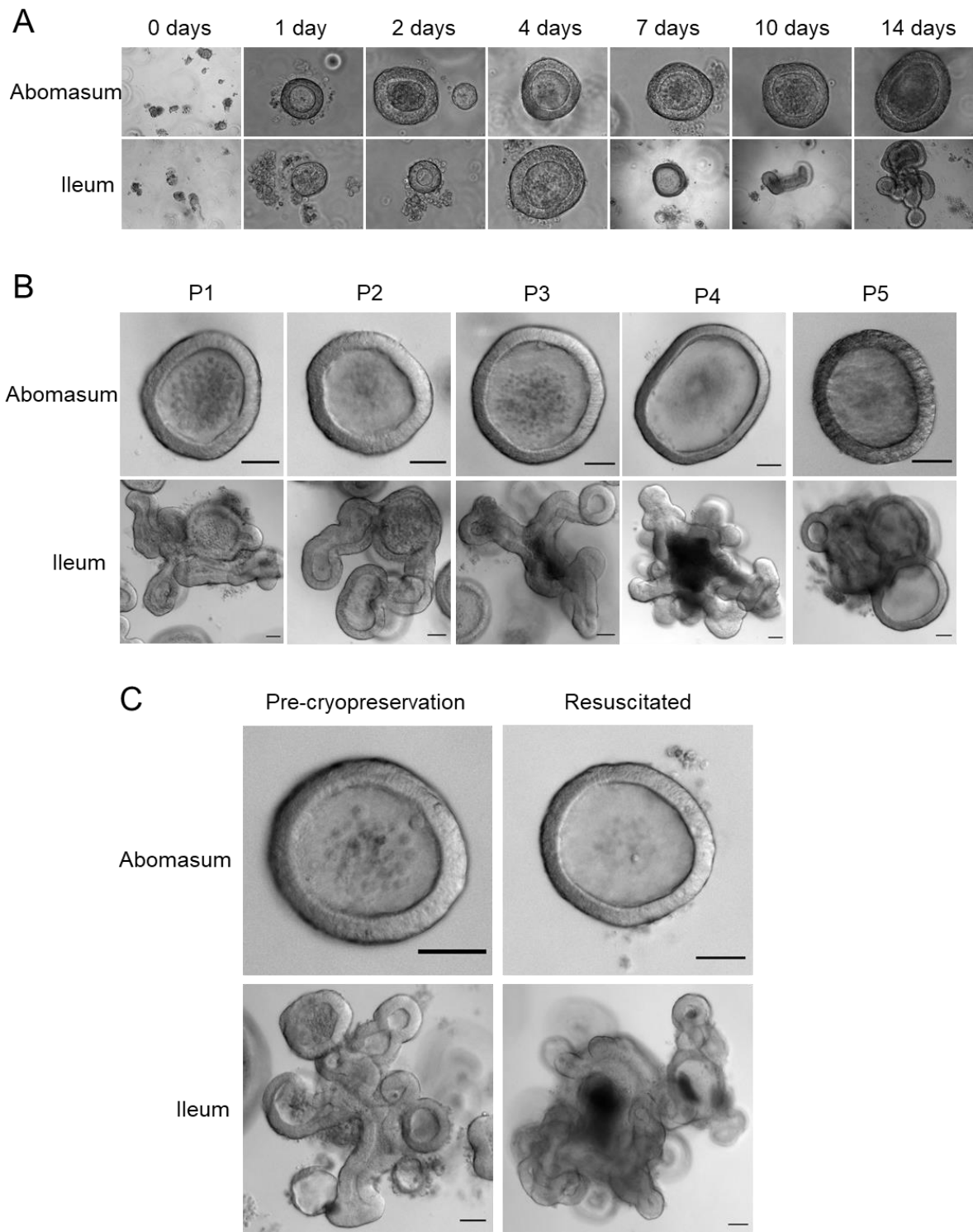900
901
902
903
904
905
906
907
908
909
910
911

912 **Figure 1**

913



914
915
916
917
918
919
920
921
922
923
924
925
926
927
928
929
930
931
932
933
934
935
936
937
938
939
940
941
942
943

944     **Figure 2**

945



946
947
948
949
950
951
952
953
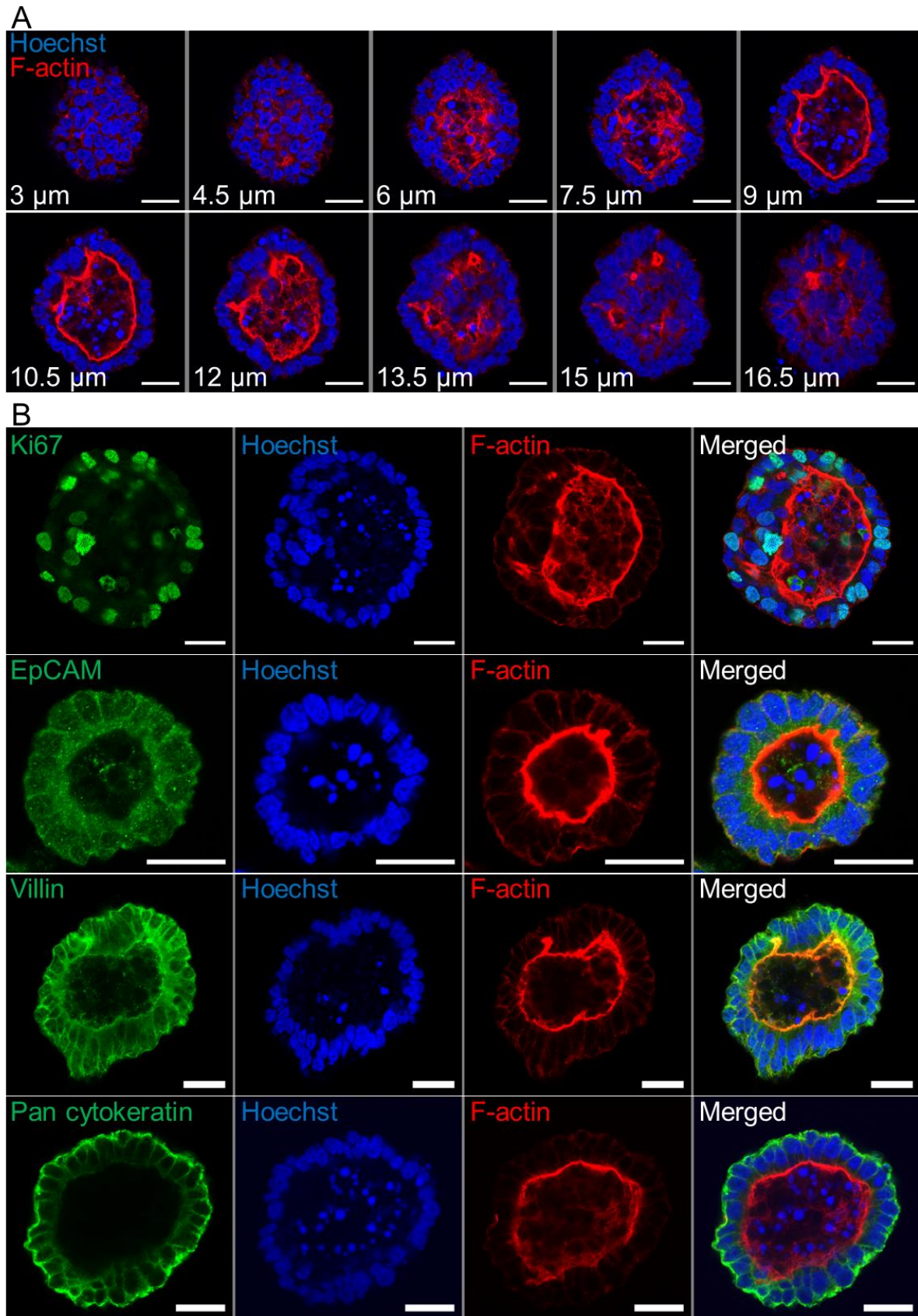
954    **Figure 3**

955



956
957
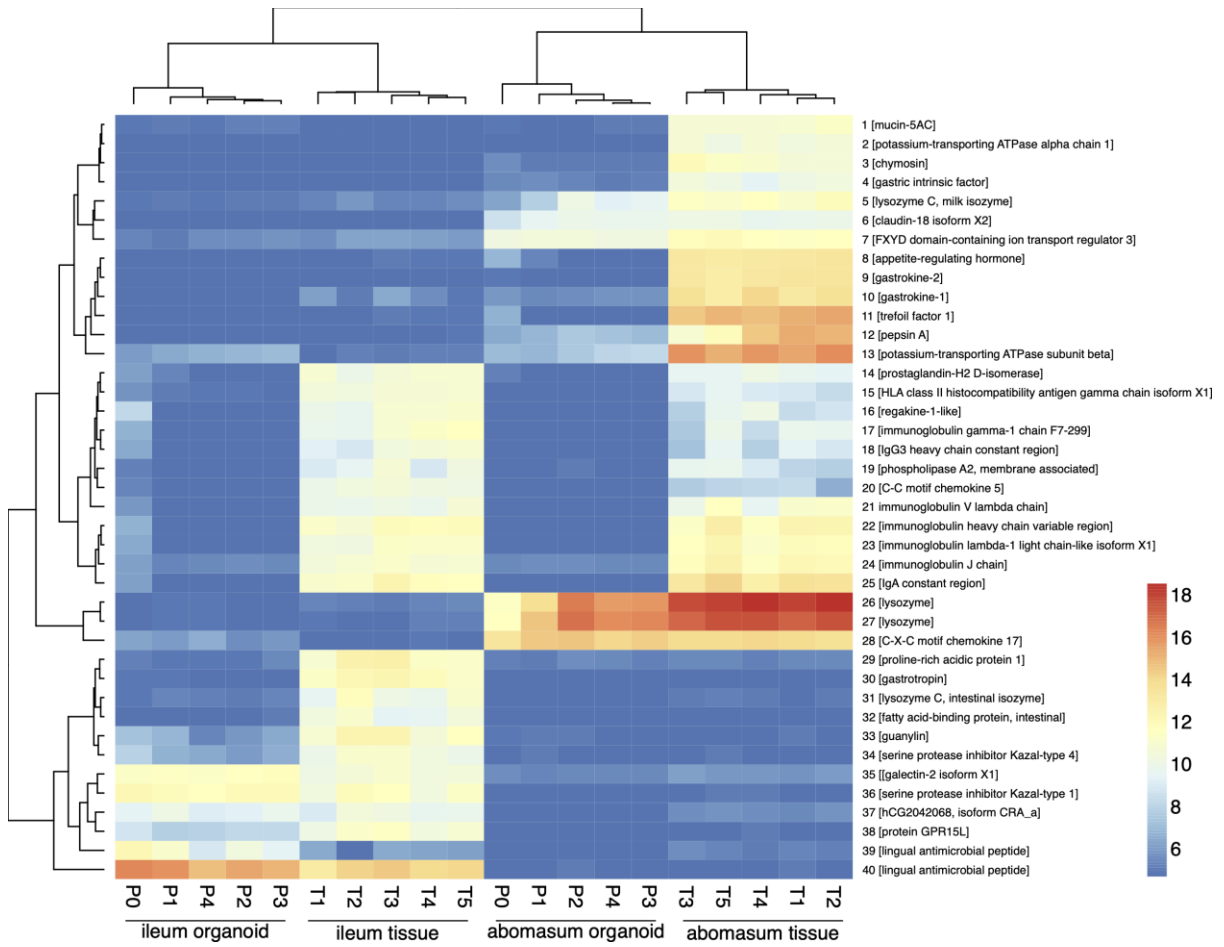
958    **Figure 4**
959



960
961
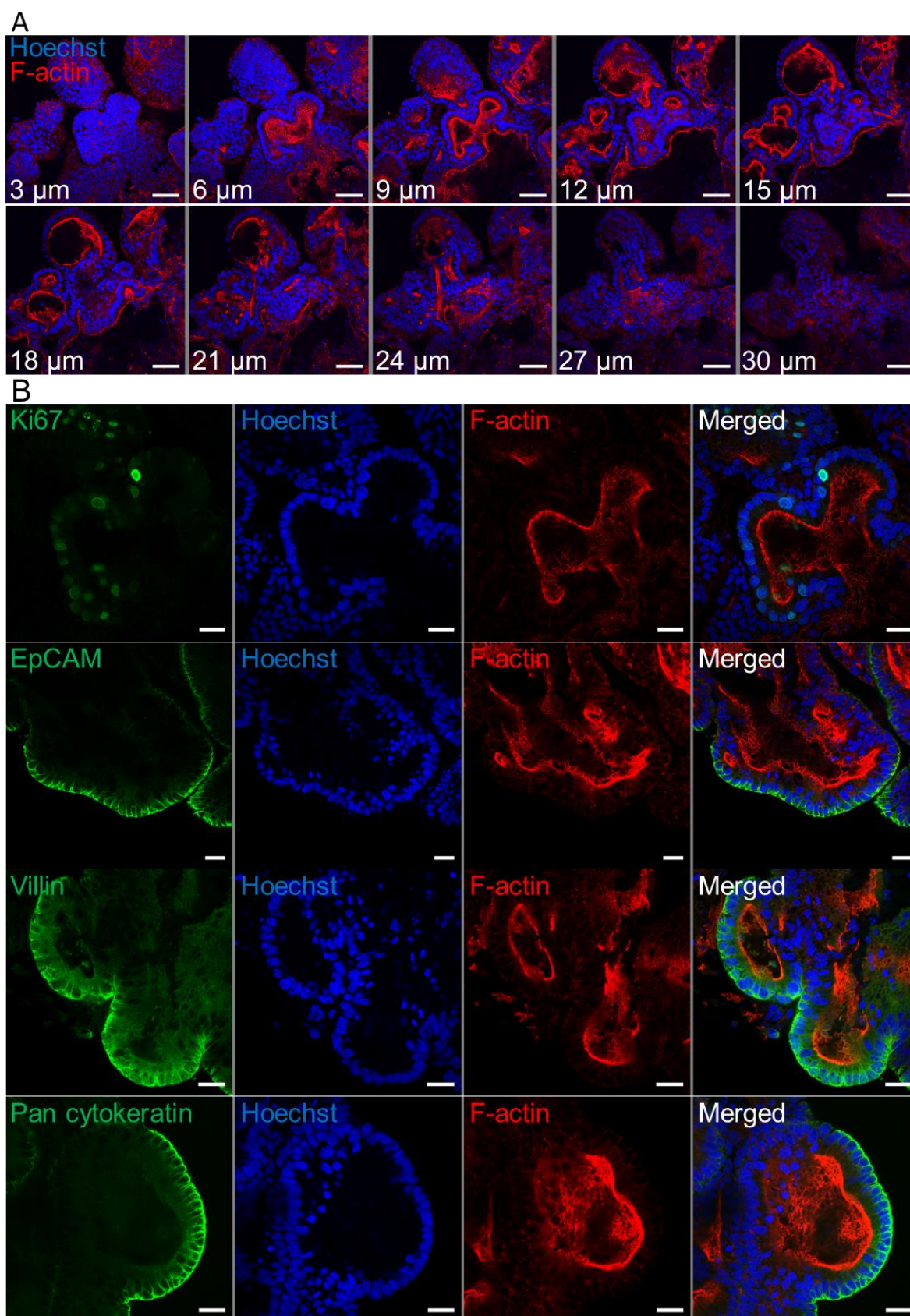
962  **Figure 5**

963
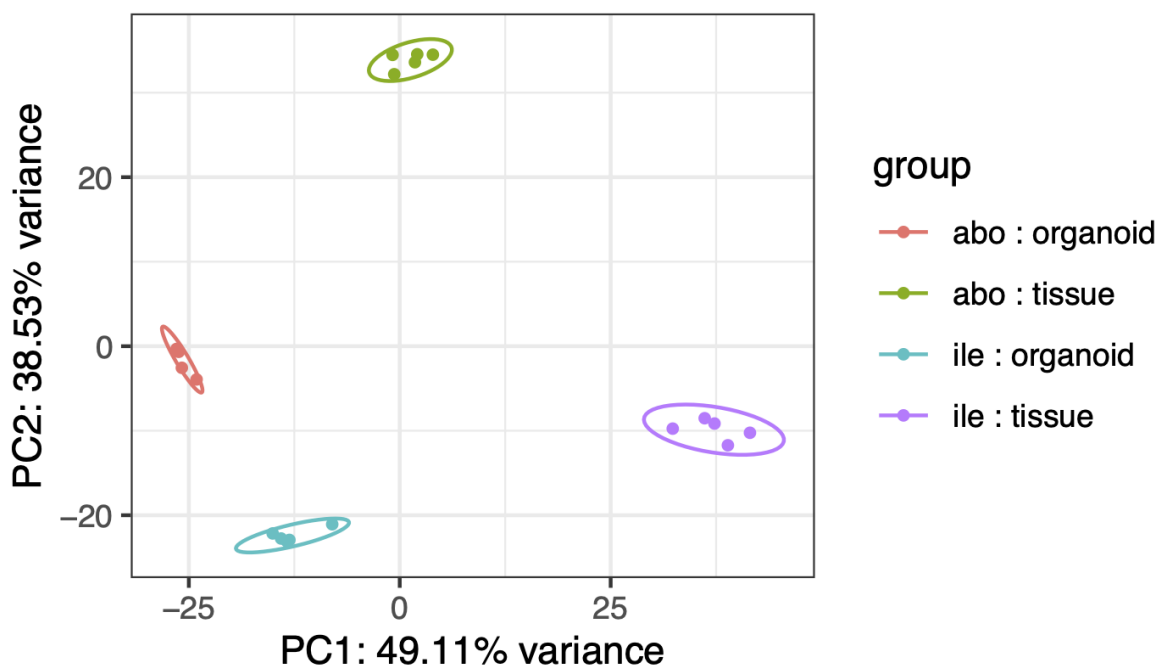


964
965
966
967
968
969
970
971
972
973
974
975
976
977
978
979
980
981
982
983
984
985
986
987
988
989
990
991

992   **Figure 6**
993



994
995
996
997
998
999
1000
1001
1002
1003
1004
1005
1006
1007
1008
1009
1010
1011
1012
1013
1014
1015
1016

1017    **Figure 7**

1018
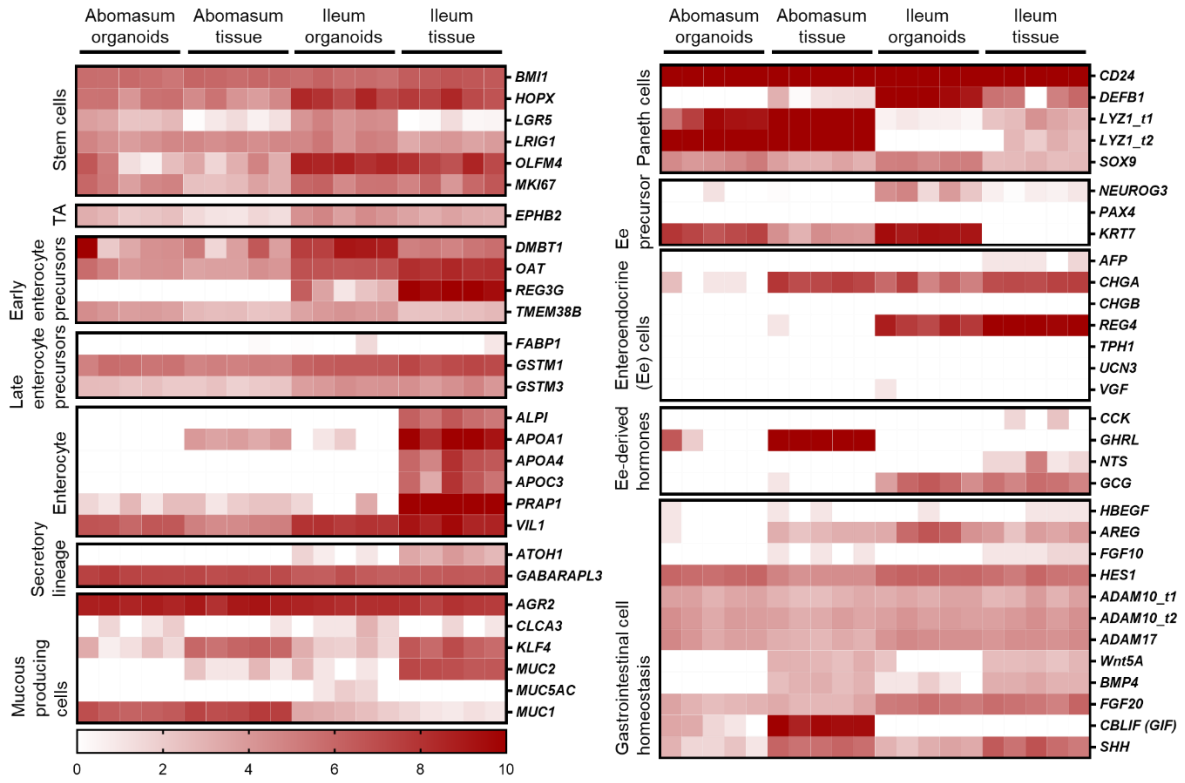


1019
1020
1021
1022
1023
1024
1025
1026
1027
1028
1029
1030
1031
1032
1033
1034
1035
1036
1037
1038
1039
1040
1041
1042
1043
1044
1045

1046  **Figure 8**
1047
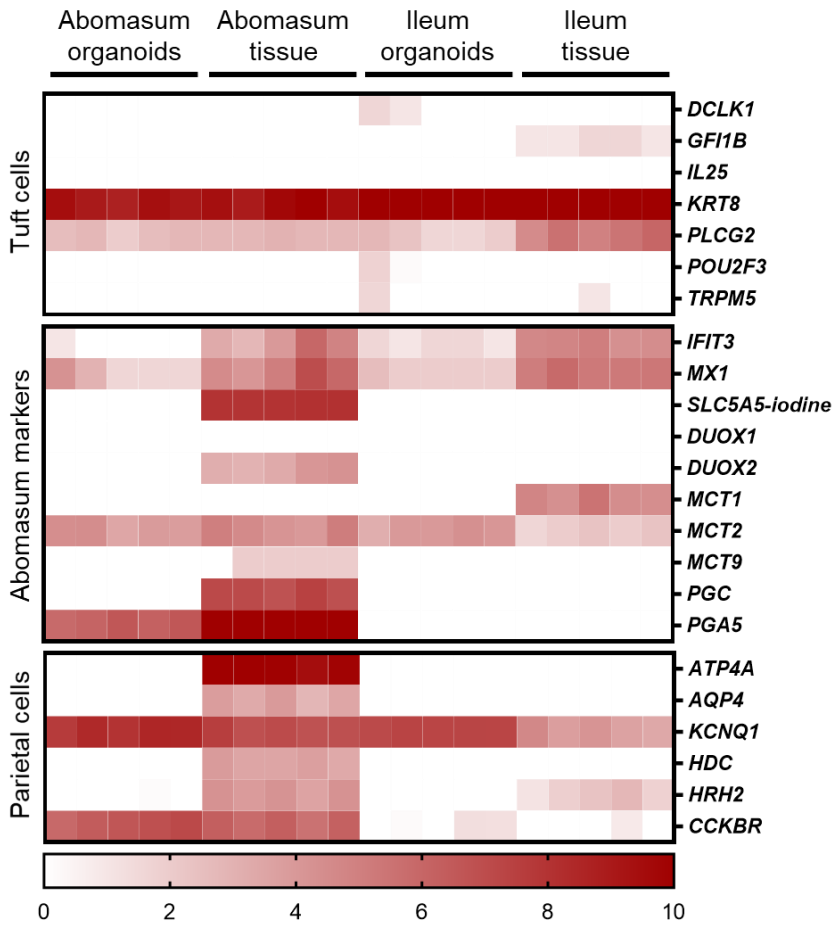


1048
1049
1050
1051
1052
1053
1054
1055
1056
1057
1058
1059
1060
1061
1062
1063
1064
1065
1066
1067
1068
1069
1070

1071    **Figure 9**
1072
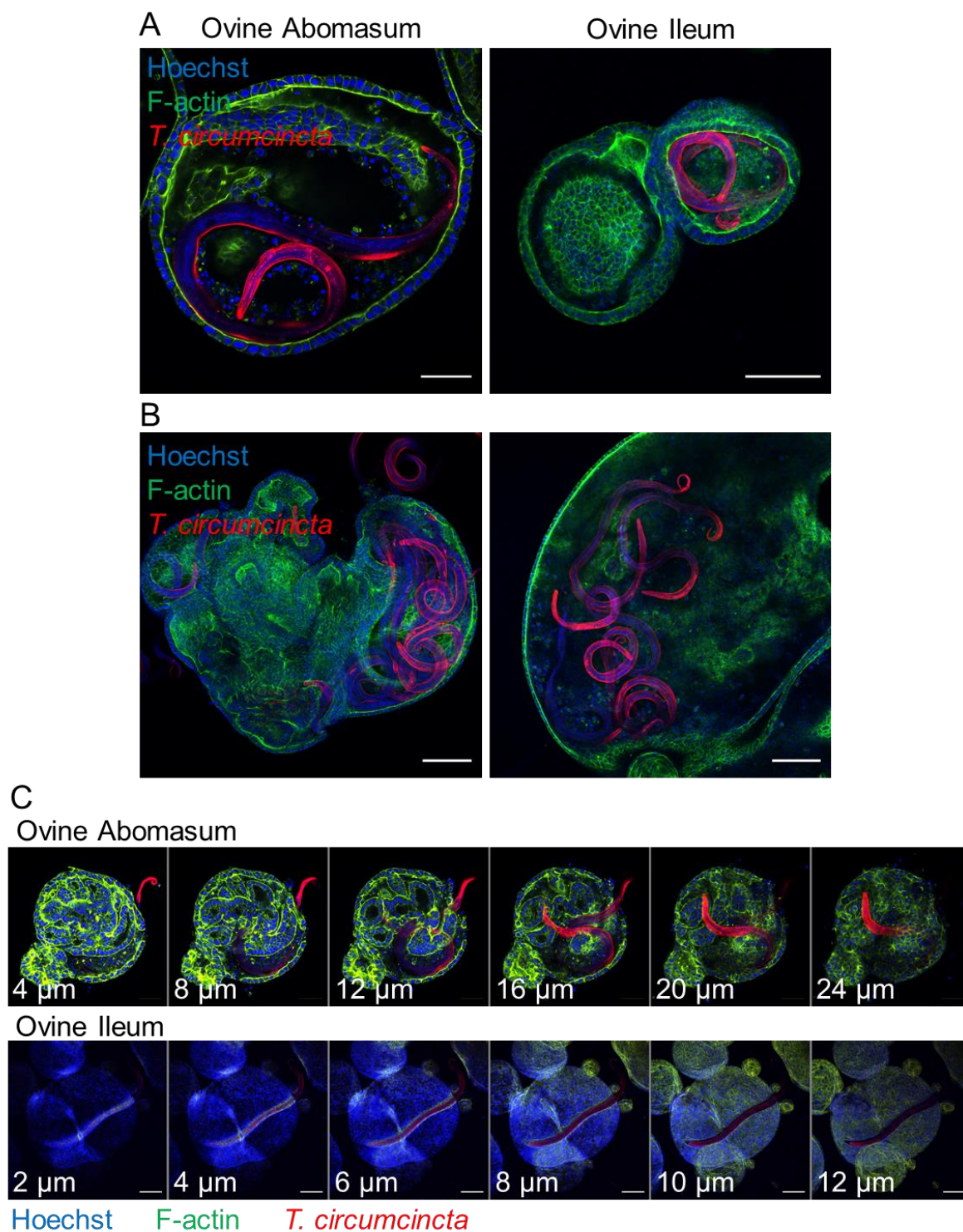


1073
1074
1075
1076
1077
1078
1079
1080

1081    **Figure 10**
1082
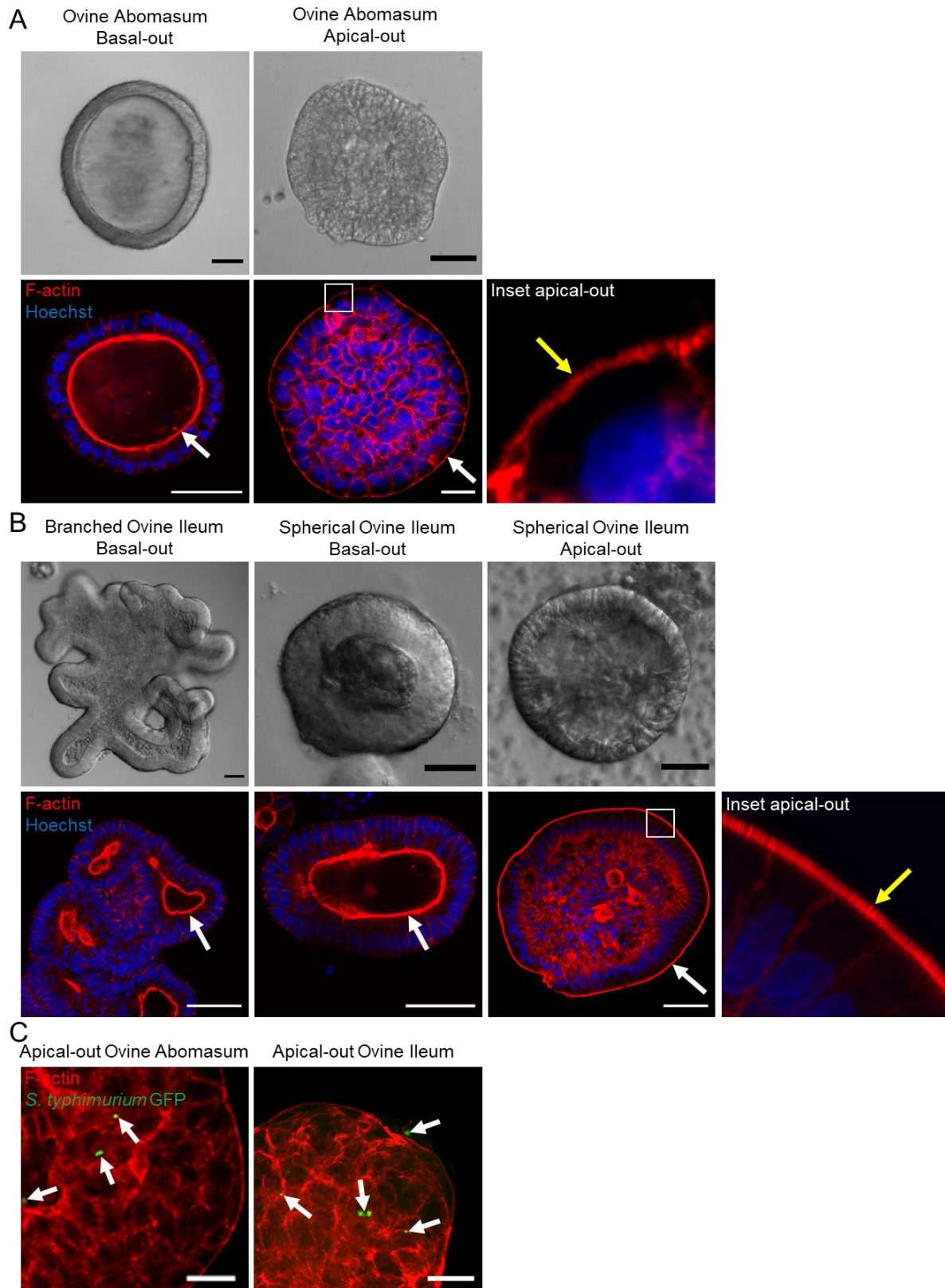


1083
1084
1085
1086
1087

1088 **Supplemental Figure 1**
1089
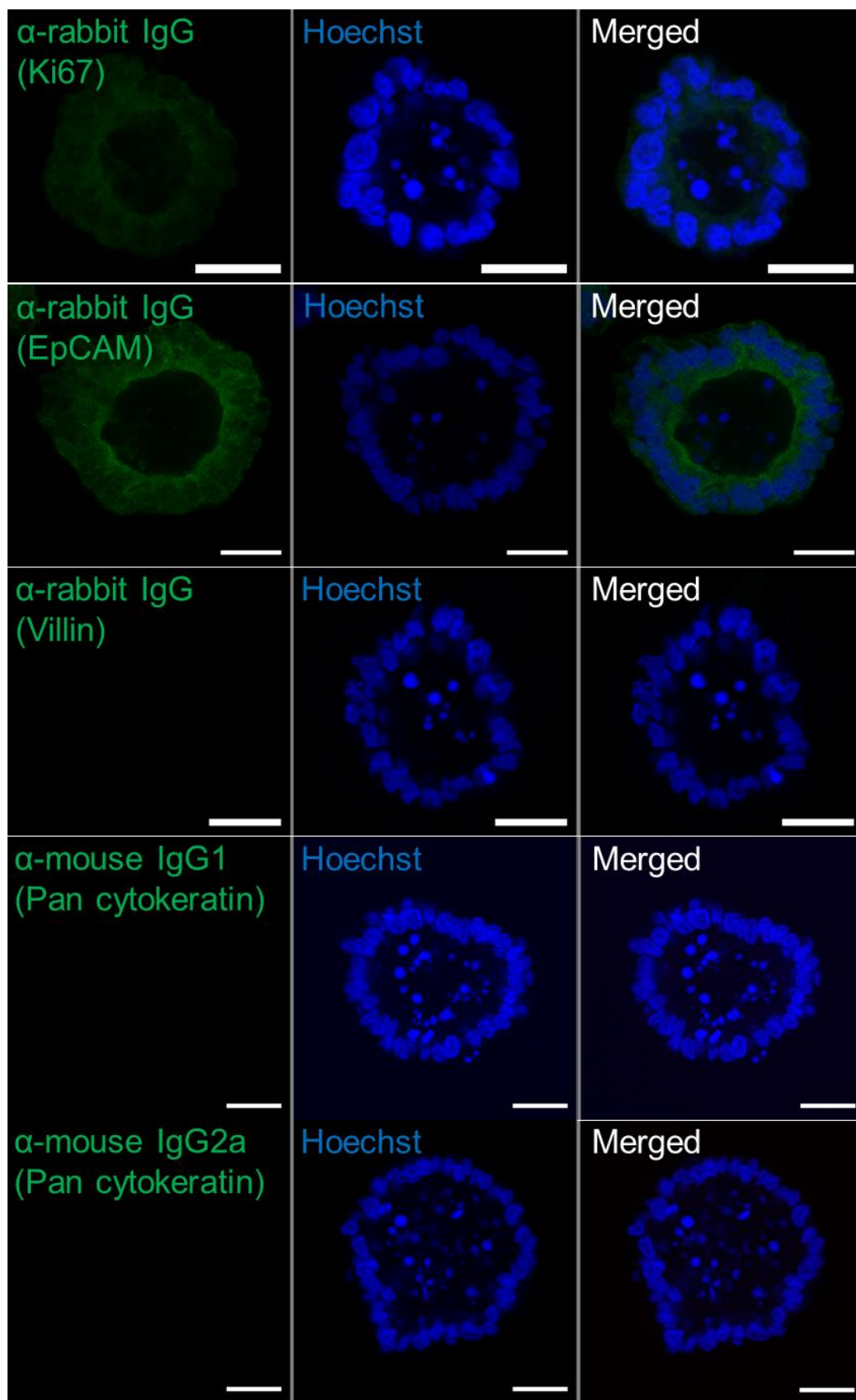


1090
1091
1092

1093    **Supplementary Figure 2**

1094
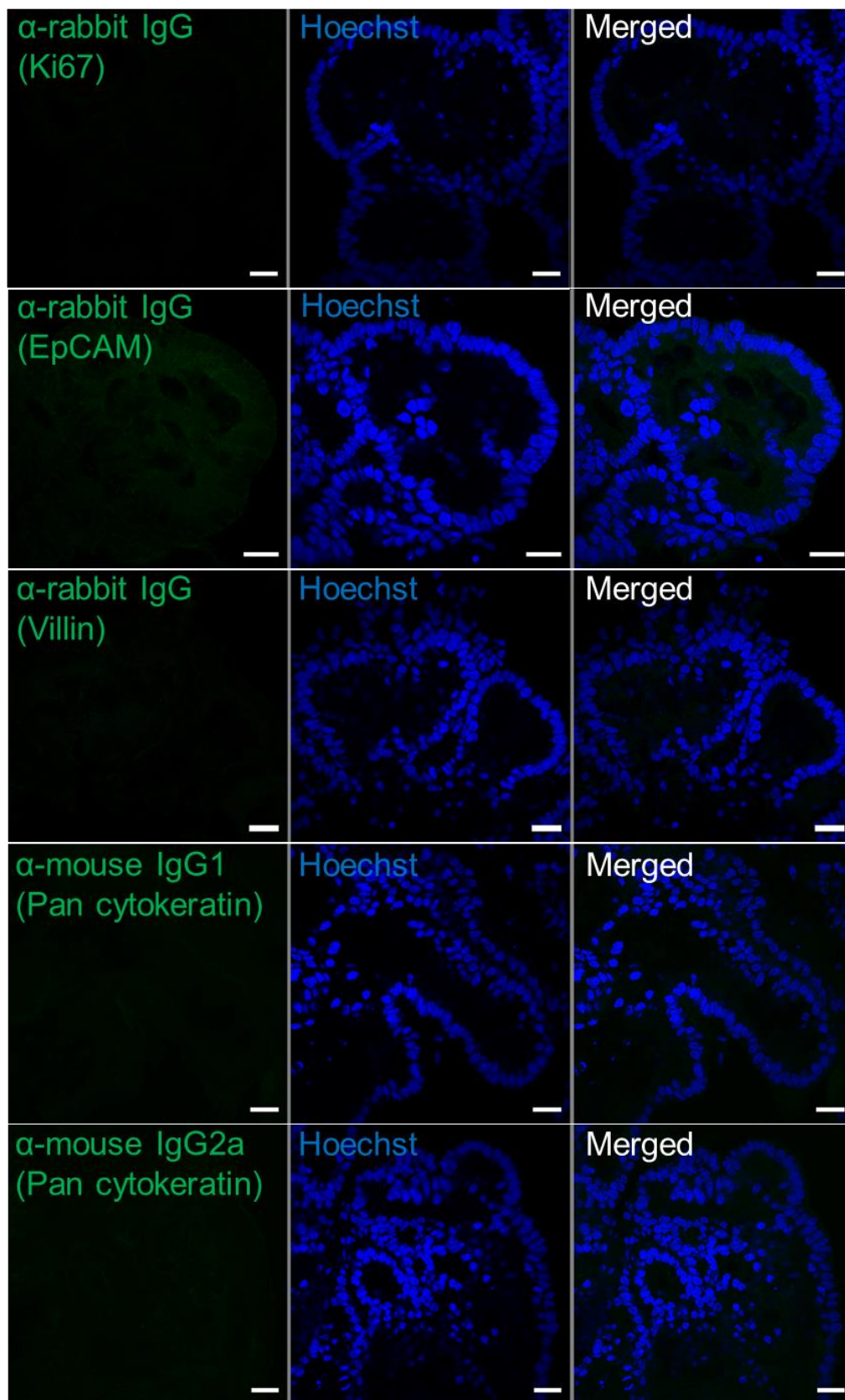


1095
1096
1097

1098    **Supplementary Figure 3**

1099
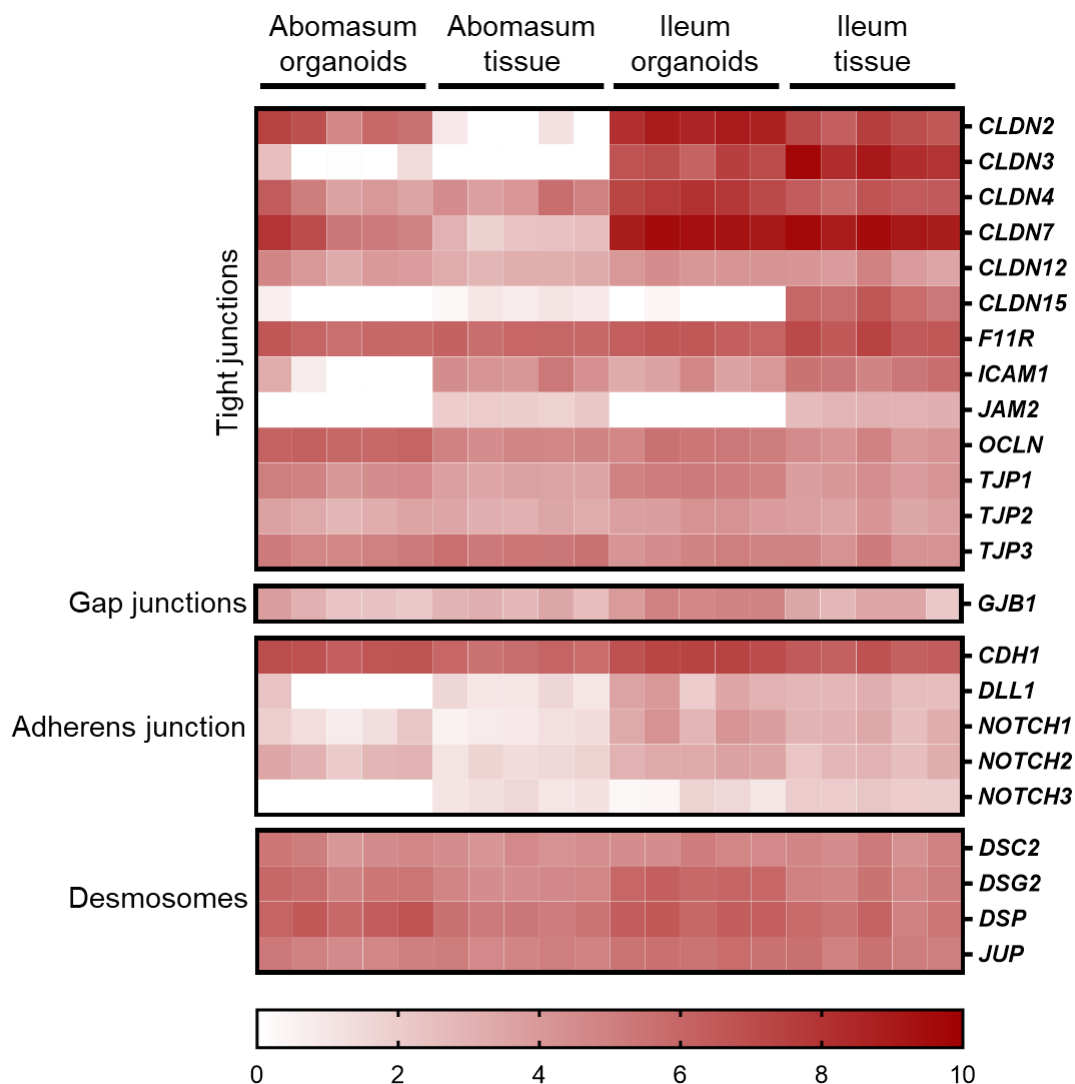


1100
1101
1102
1103
1104
1105
1106
1107
1108
1109
1110
1111
1112
1113
1114
1115
1116
1117
1118

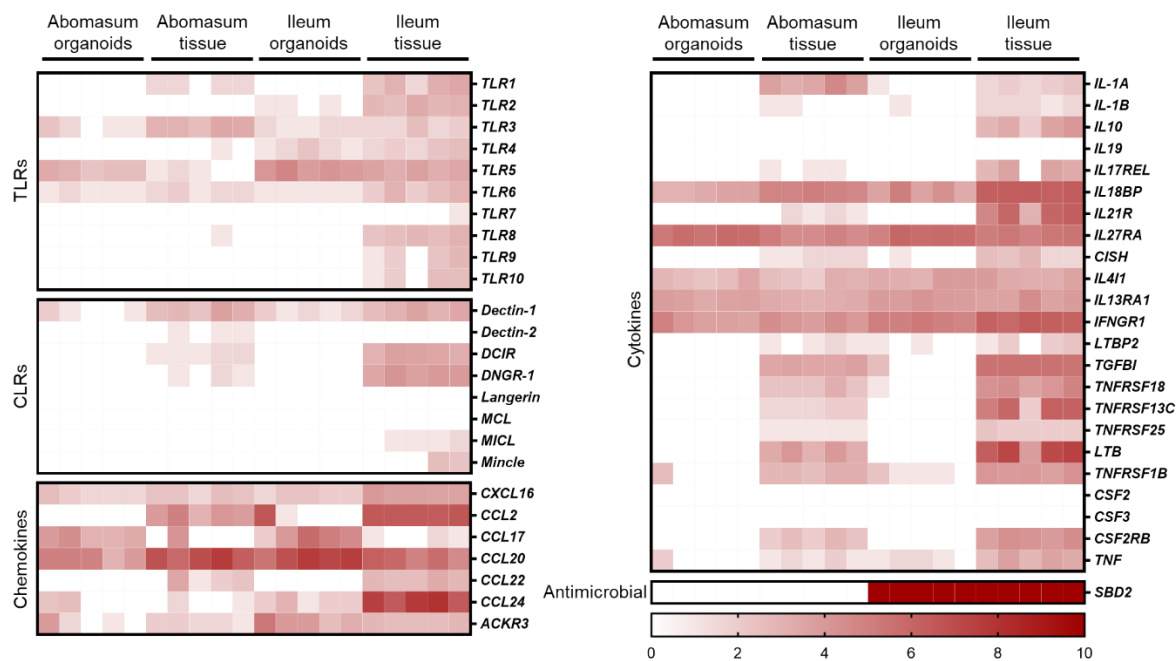1119 **Supplementary Figure 4**

1120



1121